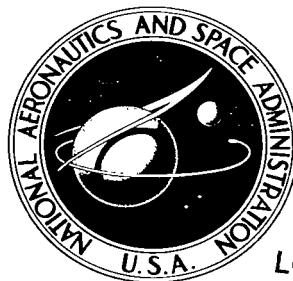


NASA TECHNICAL
REPORT



NASA TR R-168

21

LOAN COPY: RE
AFWL (WLI)
KIRTLAND AFB,

0068087



TECH LIBRARY KAFB, NM

NASA TR R-168

DIRECTIONAL DEPENDENCE OF
COUNTING RATES FROM EXPLORER IV
(SATELLITE 1958 EPSILON)

by Robert Jordan Naumann

*George C. Marshall Space Flight Center
Huntsville, Ala.*



DIRECTIONAL DEPENDENCE OF
COUNTING RATES FROM EXPLORER IV

(SATELLITE 1958 EPSILON)

By Robert Jordan Naumann

George C. Marshall Space Flight Center
Huntsville, Ala.

NATIONAL AERONAUTICS AND SPACE ADMINISTRATION

For sale by the Office of Technical Services, Department of Commerce,
Washington, D.C. 20230 -- Price \$2.00



TABLE OF CONTENTS

	Page
SECTION I.	
INTRODUCTION	2
A. Theory of Particle Trapping in Magnetic Fields	3
B. Observations of Trapped Radiation	5
C. Anisotropy of Trapped Radiation	6
D. Description of the Scintillation Detector	7
E. General Description of the Rigid Body Motion of Satellite 1958 Epsilon	9
SECTION II.	
DETERMINATION OF THE TUMBLE AXIS	17
A. Discussion of the Tumble Axis Determination	17
B. Confirmation of the Tumble Axis Determination	34
SECTION III.	
DETERMINING COUNTER ORIENTATION	42
SECTION IV.	
RESULTS AND CONCLUSIONS	50
A. Analysis of Observed Radiation	50
B. Error Analysis	51
C. Conclusions	62
APPENDIX 1	64
APPENDIX 2	65

LIST OF ILLUSTRATIONS

Figure	Title	Page
1.	Explorer IV Payload Configuration Showing the Placement of the Directional Scintillation detectors	8
2.	Telemetry Sample Showing the Variations in the Channel 2 Counting Rates Due to the Body Motions of Explorer IV	10
3.	Explorer IV External Configuration and Dynamical Properties	11
4.	Observed Roll Period During the Telemetry Lifetime of Explorer IV	13
5.	Explorer IV Temperatures Measured During Transmitter Lifetime from the Channel 3 Subcarrier Frequency	15
6.	Calculated Temperatures for Explorer IV for Various Fractions of the Longitudinal Area Presented to the Sun	16
7.	Explorer IV Antenna Radiation Patterns	18
8.	Right Ascension and Declination of the Sight Vector for Passes During August 12, 1958	20
9.	Right Ascension and Declination of the Sight Vector for August 18, 1958	21
10.	Telemetry Sample Showing the 108.03 mc/sec Signal Strength Variations for $\Psi < 30^\circ$	23
11.	Telemetry Sample Illustrating the Signal Strength Variations for the Case of $30^\circ < \Psi < 45^\circ$	24
12.	Telemetry Sample Illustrating the Signal Strength Variations for the Case of $45^\circ < \Psi < 60^\circ$	25
13.	Telemetry Sample Illustrating the Signal Variation for the Case of $60^\circ < \Psi < 75^\circ$	26
14.	Telemetry Sample Illustrating the Signal Strength Variations for the Case of $75^\circ < \Psi < 90^\circ$	27

LIST OF ILLUSTRATIONS (Cont'd)

Figure	Title	Page
15.	Right Ascension and Declination of the Sight Vector for Passes During August 20, 1958	28
16.	Right Ascension and Declination of the Sight Vector for Passes During August 27, 1958	29
17.	Right Ascension and Declination of the Sight Vector for Passes During August 30, 1958	30
18.	Right Ascension and Declination of the Sight Vector for Passes During September 3, 1958	31
19.	Right Ascension and Declination of the Sight Vector for Passes During September 10, 1958	32
20.	Right Ascension and Declination of the Sight Vector for Passes During September 14, 1958	33
21.	Right Ascension and Declination of the Sight Vector for August 9, 1958 at times when Fading was not Observed in the Telemetry Received by the Johnston Island Station	35
22.	Right Ascension and Declination of the Sight Vector at times Fading was absent from Johnston Island Telemetry on August 11, 1958	36
23.	Polynomial Description of the Right Ascension and Declination of the Angular Momentum Vector	37
24.	Comparison of Calculated Temperature with Observed Temperature.	38
25.	Changes in Orbital Period of Explorer IV Observed by Lautman at Smithsonian Astrophysical Observatory	40
26.	Comparison of Calculated Effective Drag Area with Observed Drag Deceleration	41
27.	Observed Tumble Rate from August 27 through September 1	46

LIST OF ILLUSTRATIONS (Cont'd)

Figure	Title	Page
28.	Geometry of a Typical Pass at Acquisition During the Period from August 27 to September 1	48
29.	Comparison of Observed Counting Rates with the Calculated λ During the Interval 0500:00 to 0500:30 UT on August 30, 1958	52
30.	Comparison of Observed Counting Rates with the Calculated λ During the Interval 0500:30 to 0501:00 UT on August 30, 1958	53
31.	Comparison of Observed Counting Rates with the Calculated λ During the Interval 0510:00 to 0510:30 UT on August, 1958	54
32.	Counting Rate Versus λ for 0500:00 to 0500:30 UT, August 30, 1958 .	55
33.	Counting Rate Versus λ for 0500:30 to 0501:00 UT, August 30, 1958 .	56
34.	Counting Rate Versus λ for 0501:00 to 0501:30 UT, August 30, 1958 .	57
35.	Counting Rate Versus λ for 0501:30 to 0502:00 UT, August 30, 1958 .	58
36.	Counting Rate Versus λ for 0502:30 to 0503:00 UT, August 30, 1958 .	59
37.	Counting Rate Versus λ for 0510:07 to 0510:25 UT, August 30, 1958 .	60

TECHNICAL REPORT R-168

DIRECTIONAL DEPENDENCE OF
COUNTING RATES FROM EXPLORER IV
(Satellite 1958 Epsilon)

by

Robert Jordan Naumann

SUMMARY

Inspection of the directional scintillation counter data from Explorer IV revealed fluctuations in the counting rate that appeared to be due to the body motions of the satellite and the anisotropy of the radiation flux. It was felt that the body motions and the angular dependence of the radiation flux could be determined from the data available.

This work is a description of the methods used and results obtained from this determination. It was found that the counting rate is generally a maximum when the detector axis is normal to the magnetic field which is expected from the theory of particle trapping. The counting rate falls off as the detector axis makes smaller angles with the magnetic field lines, reaching a minimum value when the detector comes within about 40 degrees of the magnetic field lines. Knowledge of this angular dependence of the counting rate will allow calculation of the radiation distribution along a particular magnetic line of force.

In the analysis of the rigid body motion, two rather surprising facts were observed. First, the components of the total angular momentum vector of the satellite do not remain constant in a space orientation-fixed reference system, although the magnitude remains essentially constant. Second, the small residual roll of the satellite about its longitudinal axis does not decay monotonically. In fact, at one point, the roll rate was observed to increase by almost an order of magnitude in one day. These two observations suggest that external forces are present and exert body torques on the satellite. It is possible that the origin of the forces may be due to an interaction of a magnetic moment in the satellite with the geomagnetic field, although this is not yet confirmed.

SECTION I. INTRODUCTION

One of the most significant contributions from the satellite and space program during the International Geophysical Year was the discovery of the two radiation belts encircling the earth. While much has been learned about the configuration, composition, and radiation intensities of these belts, comparatively little is known about the angular distribution of particle flux about magnetic lines of force. It is known that the radiation exhibits a strong anisotropy, but a detailed knowledge of intensity as a function of angle relative to geomagnetic field lines will aid considerably in interpreting some of the observed results and in mapping the radiation belt.

Satellite 1958 Epsilon, launched on July 26, 1958, contained two highly directional scintillation detectors as part of its radiation experiment. The rigid body motion of this satellite was such that the detector axes traced out complex motions on a unit sphere centered at the satellite, thus providing excellent directional sampling of the radiation intensity.

The purpose of this paper is to analyze and describe the rigid body motion of this satellite, finally obtaining the angle that the counter axes make with the magnetic field lines as a function of time. This angle is then correlated with observed counting rates resulting in plots of counting rate versus angle that the detector makes with the magnetic field.

The scope of this paper will be limited to obtaining these counting rate plots. The intensity as a function of angle may be determined by solving an integral equation containing these observed count rates and the angular response of the counter for various energies. This latter input awaits the completion of a new detailed calibration presently being undertaken by Baicy at the Ballistic Research Laboratories, Aberdeen, Maryland.

The first chapter of this paper is of an introductory nature giving a brief resume and history of the radiation belts as well as some characteristics of the satellite pertinent to the analysis. This is followed by the determination of the total angular momentum vector configuration from antenna patterns. It is shown that body torques apparently are acting on the satellite to produce changes in the space-fixed components of the angular momentum vector. Verification of this determination is obtained by a confirmation of the anomalous temperature fluctuations and drag variations which are explained by this analysis. Finally the counter orientation is obtained at various times of interest and the corresponding counting rates are plotted as a function of angle between the counter axis and the magnetic field.

The author wishes to express his most sincere appreciation to Dr. Charles A. Lundquist for his help and encouragement in carrying out this study. Also the author is indebted to Stanley Fields for his help in analyzing the radiation data, to Fred Rodrigue, and others, in the Computation Division for the computer programs necessary for this analysis, to Gerhard Heller and William Snoddy for the temperature analysis, and to the many others who assisted in obtaining the telemetry records and other information pertinent to this study.

A. THEORY OF PARTICLE TRAPPING IN MAGNETIC FIELDS

An intensive study of the influence of the geomagnetic field on cosmic particles was undertaken by Stormer [Ref. 1] and Alfven [Ref. 2]. While these works contain all the fundamental concepts necessary to understand the trapping of particles in the geomagnetic field near the earth, no obvious method for the injection of such particles was then apparent; hence Stormer and Alfven were primarily concerned with the motions of particles of extraterrestrial origin with high magnetic rigidities. Interest in magnetic trapping of charged particles was stimulated by attempts to confine high temperature plasmas with the hope of obtaining thermonuclear reactions. The magnetic mirror concept, although not by any means new (dating back to Poincare), is presented very clearly by Spitzer [Ref. 3] and would be worthwhile to review at this point.

Consider a particle with mass m and charge q moving with velocity \vec{v} in a uniform magnetic field \vec{B} . The basic equation of motion is

$$m \frac{d\vec{v}}{dt} = q (\vec{v} \times \vec{B}). \quad (1)$$

If \vec{v} is resolved into a component v_{\perp} perpendicular to \vec{B} , and a component v_{\parallel} parallel to \vec{B} , it may be seen that the force is always perpendicular to both the velocity and magnetic lines of force. This results in the particle gyrating about a point on the line of force called the guiding center. Since the v_{\parallel} component is unchanged, the guiding center will move along the line of force with velocity v_{\parallel} . The resulting motion is a helical path about the magnetic field line. The radius of gyration a and the cyclotron frequency ω_c are immediately found by equating the centrifugal force to the magnetic force exerted on the particle:

$$\text{or} \quad \frac{m v_{\perp}^2}{a} = q v_{\perp} B, \quad (2)$$

$$a = \frac{m v_{\perp}}{q B}, \quad (3)$$

$$\text{and} \quad \omega_c = \frac{v_{\perp}}{a} = \frac{q B}{m}. \quad (4)$$

The magnetic moment of the gyrating particle is the current $q \omega_c / 2\pi$ times the area encircled by the gyrating particle, πa^2 .

$$\mu = \frac{a^2 q \omega_c}{2} = \frac{m v_{\perp}^2}{2B} . \quad (5)$$

Consider the case of the spiraling particle moving into a region of greater B. Assume that the change B is small over a cross section of the particle's orbit such that $\partial B_z / \partial z$ is constant in a cylindrical coordinate system with \vec{B} along the z-axis, and is essentially equal to $\partial B / \partial z$. From

$$\nabla \cdot \vec{B} = 0, \quad (6)$$

one obtains

$$\frac{1}{r} \frac{\partial}{\partial r} (r B_r) + \frac{\partial B_z}{\partial z} = 0. \quad (7)$$

From the assumption on $\partial B_z / \partial z$, equation 7 may be integrated to give

$$B_r = - \frac{1}{2} r \frac{\partial B}{\partial z} . \quad (8)$$

Since \vec{B} is along the z-axis, denote $\partial B / \partial z = \nabla_{\parallel} B$. Since B is increasing in density, the lines of force are converging and there must exist a radial component B_r . This component through equation 1 results in a retarding force on the particle given by

$$m \frac{dv_{\parallel}}{dt} = q v_{\perp} B_r. \quad (9)$$

From equation 8 with $r = a$ and equation 9,

$$m \frac{dv_{\parallel}}{dt} = - \frac{1}{2} q v_{\perp} a \nabla_{\parallel} B = - \mu \nabla_{\parallel} B. \quad (10)$$

Using this result with equation 5 and the assumption that kinetic energy is conserved, it may be shown that the magnetic moment μ is conserved for slowly varying B (See Appendix 1). This quantity is termed an "adiabatic invariant." According to Northrop and Teller [Ref. 4] the conservation of magnetic moment as well as other adiabatic invariants holds also for relativistic particles.

The conservation of magnetic moment has the immediate consequence that particles will be reflected away from a region of increasing magnetic field [Ref. 5]. This is seen from equation 5 if the velocity vector is assumed to make angle α with the line of force B. The component v_{\perp} becomes $v \sin \alpha$ and μ becomes

$$\mu = \frac{mv^2}{2B} \sin^2 \alpha = \text{constant.} \quad (11)$$

As B increases, α also increases until $\sin \alpha = 1$. At this point, determined by the injection conditions B_0 and α_0 , the particle undergoes reflection and emerges from the region of denser B. In the geomagnetic field a particle injected with a magnetic moment such that mirroring will occur before the particle enters the denser atmosphere will continue to undergo reflections at mirror points in both hemispheres, thus becoming trapped on a line of force. Due to perturbations such as the perpendicular gradient of B, centrifugal force due to particle motion along curved lines of force, and possible due to electric fields, the particles undergo a longitudinal drift. Assuming axial symmetry of the geomagnetic field, a trapped particle must remain on a figure of revolution described by the field line on which it is trapped. The nonaxial case is also discussed by Northrop and Teller.

B. OBSERVATIONS OF TRAPPED RADIATION

Prior to 1958 the only facilities available for high altitude measurement of cosmic rays were aircraft, rockets, and balloons. The intensities observed at altitudes available to these vehicles agreed quite well with expected intensities caused by cosmic ray primaries. In the studies of auroral activity using rocket-borne radiation detectors, Van Allen and others obtained evidence that the particles responsible for the aurora may be trapped on lines of force [Ref. 6].

The launching of satellite 1958 Alpha, equipped with a State University of Iowa radiation experiment designed to detect cosmic primaries [Ref. 7], provided the first real evidence of the high intensity radiation zone beginning at 1000 kilometers above the earth at the magnetic equator. Actually in the case of 1958 Alpha, the intensity at times was so high that the counters were saturated, resulting in no observed counts [Ref. 8].

Despite this saturation effect, the observation that the radiation intensity increased rapidly in going from 700 km to 1000 km led to the conclusion that the high intensity radiation was constrained from reaching lower altitudes by the geomagnetic field; hence, the observed radiation must be charged particles trapped on magnetic lines of force. The correctness of this assumption was verified with the launchings of 1958 Gamma and Epsilon or Explorers III and IV as they are commonly called [Ref. 9].

During the telemetry lifetime of Explorer IV the Argus Experiment, suggested by Christofilos [Ref. 10], was carried out. The experiment consisted of exploding three small yield atomic devices at different times at altitudes of around 400 km near the auroral latitudes. High energy electrons resulting from the burst and from beta decay

of the fission fragments became trapped on magnetic lines of force, thus forming an "Argus shell." The configuration and intensity of this shell was then measured using Explorer IV [Ref. 11] and a series of Jason sounding rockets [Ref. 12].

Shortly after the Argus Experiment, the launching of several lunar probes made it evident that there existed a second radiation belt extending out to several earth radii [Refs. 13 through 16].

Other experiments, particularly those of Freden and White [Ref. 17] in which emulsion packs were flown and recovered in Thor nose cones, indicated that the energetic component of the inner belt was primarily due to protons. Also, it was found that the outer belt consisting of electrons is subject to temporal variations and is strongly connected with solar and auroral activity [Refs. 18, 19] while the inner belt remains relatively unvarying with time [Ref. 20].

C. ANISOTROPY OF TRAPPED RADIATION

For every point on a magnetic line of force there is some critical angle that the velocity of the particle must make with the field line if it is to be reflected before entering the dense atmosphere. Particles injected into the field with angles less than this critical value will soon be lost; hence, there should be a comparatively radiation-free cone defined by this critical angle. If a directional detector flown on a satellite is allowed to sweep through various angles with the field lines, strong variations in counting rate should be observed as the counter moves in and out of this excluded zone. If the angle that the counter axis makes with the field line can be determined at various times, this may be correlated with the observed count rate at these times resulting in a determination of the directional distribution of radiation flux. Such a determination may be useful in determining the injection mechanism for the trapped particles [Refs. 21 through 23].

This angular distribution together with the integral invariant may provide a means for mapping the entire radiation belt using a theorem developed by Northrop and Teller, that is, "In a steady state with no electric fields present, contours of constant B on an invariant surface are also contours of constant particle density [Ref. 24]."

An effort was made to determine the angular distribution of trapped particles by Welch using the data from the Jason sounding rockets. The resulting plot of count rate versus angle very closely resembled the angular response of the detector; hence, it was concluded that the intensity function was indistinguishable from a delta function at 90 degrees to the magnetic field [Ref. 25]. These data were obtained at low altitude near a mirror point.

Van Allen reports that the Argus radiation was always observed to be disc-like with an angular thickness of the order of ± 20 degrees or less [Ref. 26], and that the natural radiation appeared to be ± 30 degrees [Ref. 27].

From an examination of the Channel 2 scintillation detector telemetry and the field strength recordings taken by the Huntsville Tracking Station, it was concluded that all the information necessary to obtain a detailed determination of angular distribution of radiation flux at various magnetic latitudes was available. The task of unscrambling this information and providing this determination was then undertaken by the Author.

D. DESCRIPTION OF THE SCINTILLATION DETECTOR

The scintillation detector on Explorer IV is described by Van Allen as consisting of a plastic scintillator disc, 0.762 cm in diameter and 0.178 cm thick. It is cemented on the face of an RCA 6199 photomultiplier tube [Ref. 28]. The axis of the detector was directed perpendicularly to the axis of symmetry of the satellite and through an open hole in the wall of the stainless steel payload shell, as shown in Figure 1. This aperture was covered by 0.14 gm cm² of aluminum. The unidirectional geometrical factor¹ was 0.040 cm² steradian, which increases for stopping power greater than 1.6 gm cm² to an asymptotic value of 4.2 cm² steradian.

The collimation was such that the counter accepts the full value of incident flux of particles penetrating the aluminum window but not the steel shell for half angles up to 6 degrees. The acceptance falls linearly to zero at half angles of 19 degrees.

The over-all response of the system may be represented by

$$N = \frac{\eta}{1 - \eta \tau} \quad (12)$$

where τ is the counter dead time of 91 μ sec, η is observed counting rate, and N is true counting rate.

This detector responds to electrons greater than 680 kev, protons greater than 10 Mev, and X-rays greater than 300 kev but with low efficiency [Ref. 29].

The output from this detector is scaled by a factor of 2048 and then fed to the Channel 2 bistable subcarrier oscillator. At a signal from the scalar, the subcarrier changes from the high frequency state (602 cps) to the low frequency state (518 cps). The output from the discriminator at the receiving station is seen as a square wave

1. This factor is defined by Van Allen as the true counting rate divided by the unidirectional intensity (particles cm⁻² sec⁻¹ steradian⁻¹) and the efficiency of the detector for the particles in question.

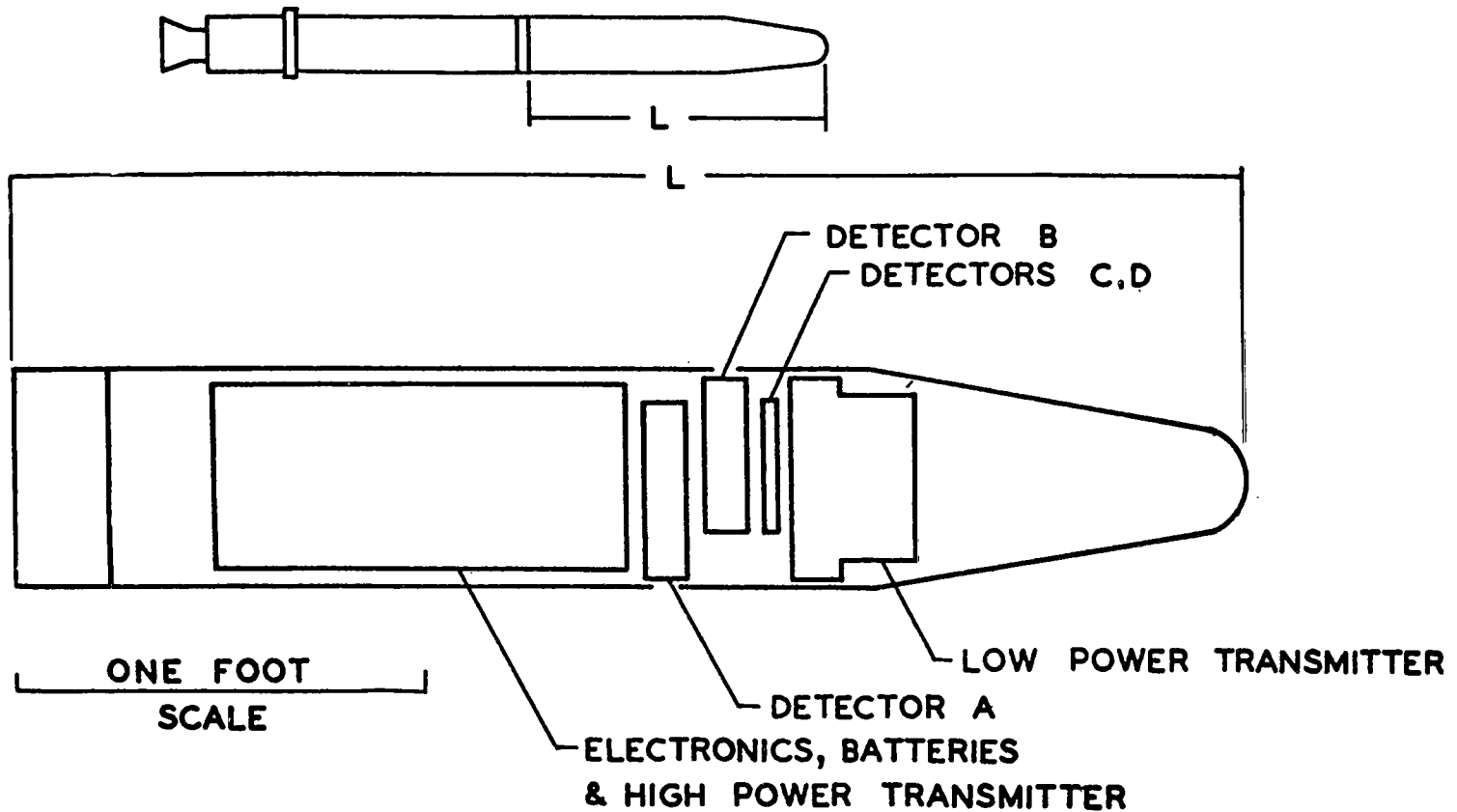


FIGURE 1. EXPLORER IV PAYLOAD CONFIGURATION SHOWING THE PLACEMENT OF THE DIRECTIONAL SCINTILLATION DETECTORS. THE CHANNEL 2 COUNTING RATES ARE THE OUTPUTS FROM DETECTOR A

with a period representing the time required to collect 2048 counts. Figure 2 is a sample of telemetry which clearly shows the effect of the satellite body motions on the Channel 2 counting rate.

E. GENERAL DESCRIPTION OF THE RIGID BODY MOTION OF SATELLITE 1958 EPSILON

The payload configuration of 1958 Epsilon is shown in Figure 3. For the purpose of discussing the rigid body motion, the satellite may be approximated by a long cylinder with a longitudinal to transverse moment of inertia ratio of 1 to 84.

Since the upper stages of the Jupiter C launching vehicle were unguided, the payload and the upper stage cluster were spun before injection to assure stability during the coast phase of the trajectory. This resulted in the payload having an initial spin of 24π rad/sec about the axis of symmetry which is the axis of least moment of inertia. Since the rotation is about the least moment of inertia, the satellite is in a maximum rotational energy configuration which is unstable for a semi-rigid body.

In the case of the earlier Explorers (I and III), a transition was observed from the axial spin at injection to a tumbling motion about a transverse axis [Ref. 30]. A detailed analysis of this transition is given by Wells [Ref. 31] for the case of Explorer I which had flexible wire turnstile antennas. This transition may be understood by considering a slight malalignment of the angular momentum and angular velocity vectors at injection. The axis of symmetry would then perform force-free precession about the angular momentum vector with precession rate $\dot{\phi}$. This precession rate may be represented by means of a Poincot construction as outlined by Goldstein [Ref. 32], or by the solution of Lagrange's equations expressed in terms of the Euler angles ϕ , θ , and ψ . This latter treatment is given by Slater and Frank in which the z-axis is taken as the direction of the total angular momentum vector, θ is the angle the figure axis of symmetry makes with the z-axis, ϕ is the angle the line of nodes makes with the space-fixed x-axis, and ψ is the angle the body-fixed x-axis makes with the line of nodes. Let the transverse moments of inertia be equal and designated by I_1 and let the longitudinal angular momentum be $I_3 \omega_3$. From equation 3.4 in Slater and Frank [Ref. 33]

$$\dot{\phi} \cos \theta = \frac{I_3}{I_1} \omega_3. \quad (13)$$

This derivation is shown in Appendix 2. From the definition of the coordinate system, the total angular momentum is related to $I_3 \omega_3$ by

$$L \cos \theta = I_3 \omega_3. \quad (14)$$

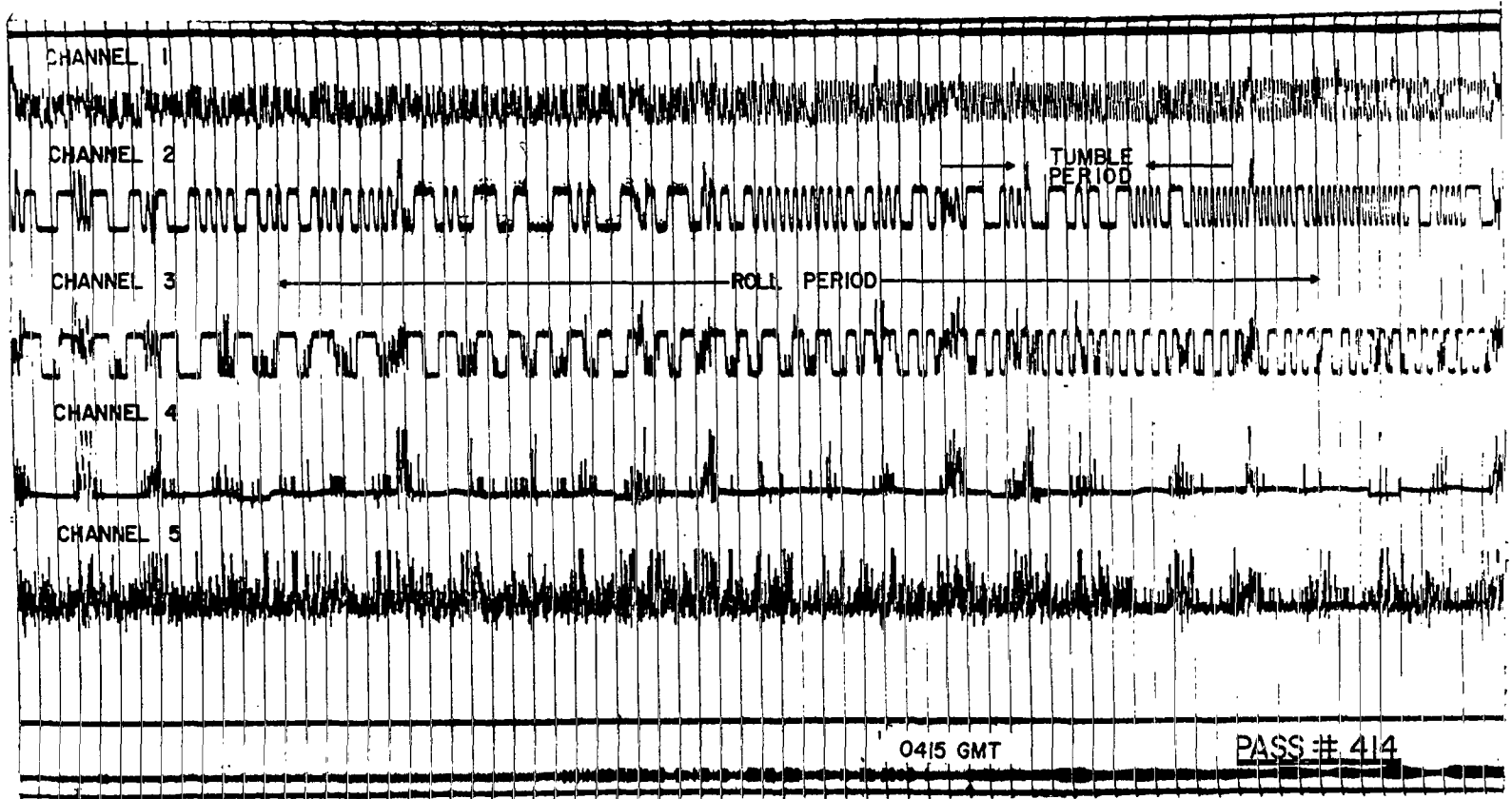


FIGURE 2. TELEMETRY SAMPLE SHOWING THE VARIATIONS IN THE CHANNEL 2 COUNTING RATES DUE TO THE BODY MOTIONS OF EXPLORER IV

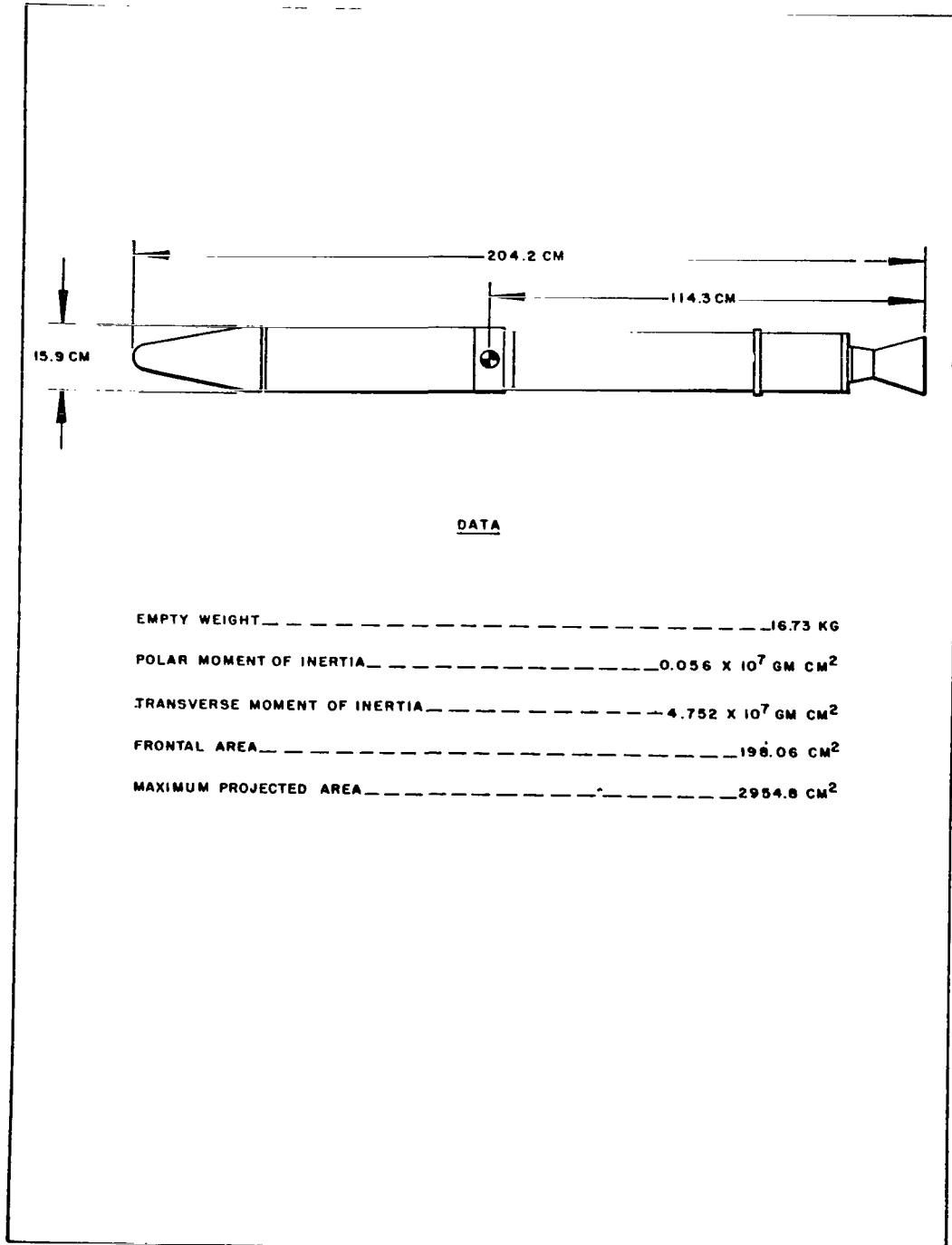


FIGURE 3. EXPLORER IV EXTERNAL CONFIGURATION AND DYNAMICAL PROPERTIES

The precession rate $\dot{\phi}$ is then found to be

$$\dot{\phi} = \frac{L}{I_1} \quad . \quad (15)$$

Initially all the angular momentum is manifested in rotation about I_3 ; hence,

$$\dot{\phi} = \frac{I_3}{I_1} \omega_3 \text{ (initial)} \quad . \quad (16)$$

With any small precession, a body-fixed mass element will experience oscillatory driving forces because of the precession rate $\dot{\phi}$ and body-fixed roll rate $\dot{\psi}$.

Unless the body is completely rigid, this mass element will be driven in forced oscillation resulting in a dissipation of rotational energy through frictional losses. Since no external torques have acted on the body, L must be a constant of the motion while rotational energy is lost. Therefore, the body must rotate about a greater moment of inertia as ω_3 decreases. Since from equation 14 $\dot{\phi}$ is constant as long as L is conserved, it is seen from equation 13 that $\cos \theta$ decreases with ω_3 . Consequently, the opening angle or the angle between the axis of symmetry and L increases with decreasing energy. Eventually this angle approaches 90 degrees, the roll rate goes to zero, and the driving forces vanish. The body is then in the stable or minimum energy configuration, and is tumbling, propeller-like, about the initial angular momentum vector which will also be referred to as the tumble axis.

The rate at which this transition takes place may be calculated if the dissipation function is known. In the case of Explorer I, the whip antennas were by far the largest contributor to the energy dissipation and were successfully treated as damped pendulums. However, in Explorer IV, the dissipation mechanism is not so obvious since efforts were made to make this payload as completely rigid as possible. Nevertheless, after several days of orbiting, evidence of tumbling was observed as the antenna power pattern nulls along the nose and tail [Ref. 34] produced periodic fades in the recorded field strength at 3.5-second intervals. Since the moment of inertia was 1 to 84 and initial roll rate was 24π rad/sec, this fading period corresponded to half the precessional period.

Since the antenna pattern was virtually symmetrical about the polar axis, it was not possible to obtain roll rate from radio observations. However, roll rate could be ascertained from the disc-like character of the trapped corpuscular radiation and the counting rate modulations of the directional counter. Such a study was performed by Fields [Ref. 35] resulting in the roll period history shown in Figure 4. From this result and equation 13, it may be seen that the opening angle had become 80 degrees after five days of orbiting. Note also that the roll never goes to zero; in fact, it is not even a monotonic decreasing function. The anomalous fluctuations on August 28 and 29

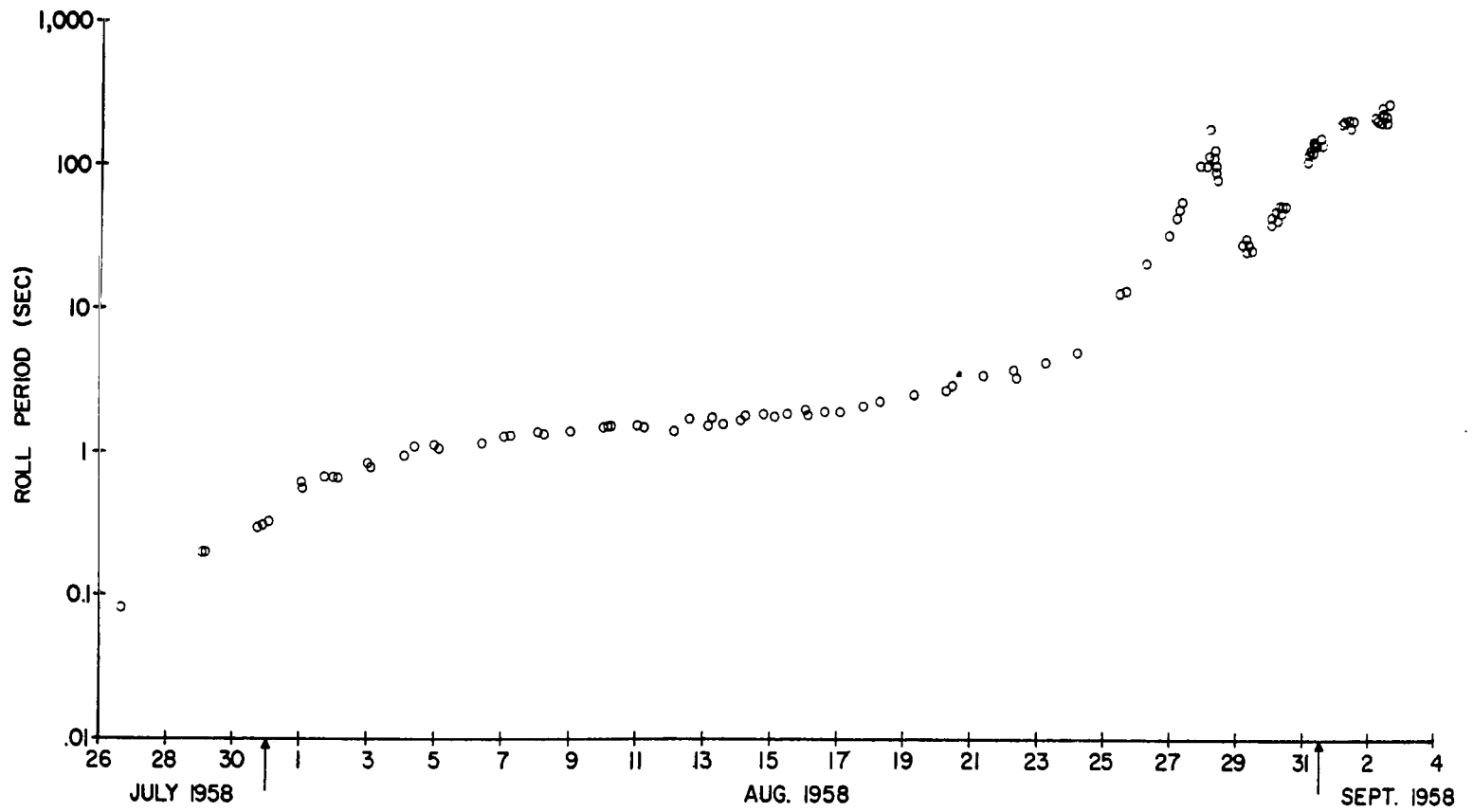


FIGURE 4. OBSERVED ROLL PERIOD DURING THE TELEMETRY LIFETIME OF EXPLORER IV

may be due to external torques which somehow have come into play. Even with a slight residual roll rate, the roll angular momentum can be neglected compared to the tumble angular momentum, and for all practical purposes the opening angle can be considered to be 90 degrees after August 1.

To determine the counter orientation, the first task is to specify the tumble axis in some inertial coordinate system. At injection, the angular momentum vector is directed along the velocity vector whose components are known in an inertial reference frame; hence, the initial tumble axis is given. Under the assumption that no external torques act on the satellite, the orientation of tumble axis would remain fixed in space. However, evidence to the contrary is reported by Snoddy through measurement of the temperature of the satellite interior [Refs. 36, 37]. Figure 5 is a history of the interior temperature obtained from the high and low frequency states of the Channel 3 subcarrier oscillator. The temperature dependence of this subcarrier oscillator frequency was determined by preflight calibration by Ludwig at the State University of Iowa. The initial drop in temperature may be attributed to the transition from axial spin, with the sun at almost a right angle to the symmetry axis, to the state of tumble where the insolated area time averaged over a tumble cycle is only 63.7 per cent of the longitudinal cross-sectional area. This decrease in insolated area results in less heat input and a lower equilibrium temperature. The fluctuations in temperature after the initial drop are difficult to explain except in terms of varying insolated area. Knowledge of the thermal properties of the satellite and of the position of the orbit relative to the earth and sun allow calculation of the expected temperatures for various percentages of insolated areas. The results of these calculations performed by Snoddy are shown in Figure 6. The maximum and minimum measured temperatures fall almost within the limits of the expected values for insolated areas ranging from 1 to .65 of the longitudinal cross section. This is strong evidence that the orientation of the plane of tumble is changing relative to the sun. The motion of the sun can account for a change of approximately one degree per day, but the area change needed to explain the temperature data demands an orientation change of 90 degrees in about 9 days, or an average change on the order of 10 degrees per day.

Throughout the telemetry lifetime of the satellite, the tumble period was observed to be very close to 3.5 seconds. Therefore, it appears that angular momentum is conserved in magnitude, but that through some mechanism, non-dissipative external torques are acting on the satellite to produce a change in the orientation of the angular momentum vector.

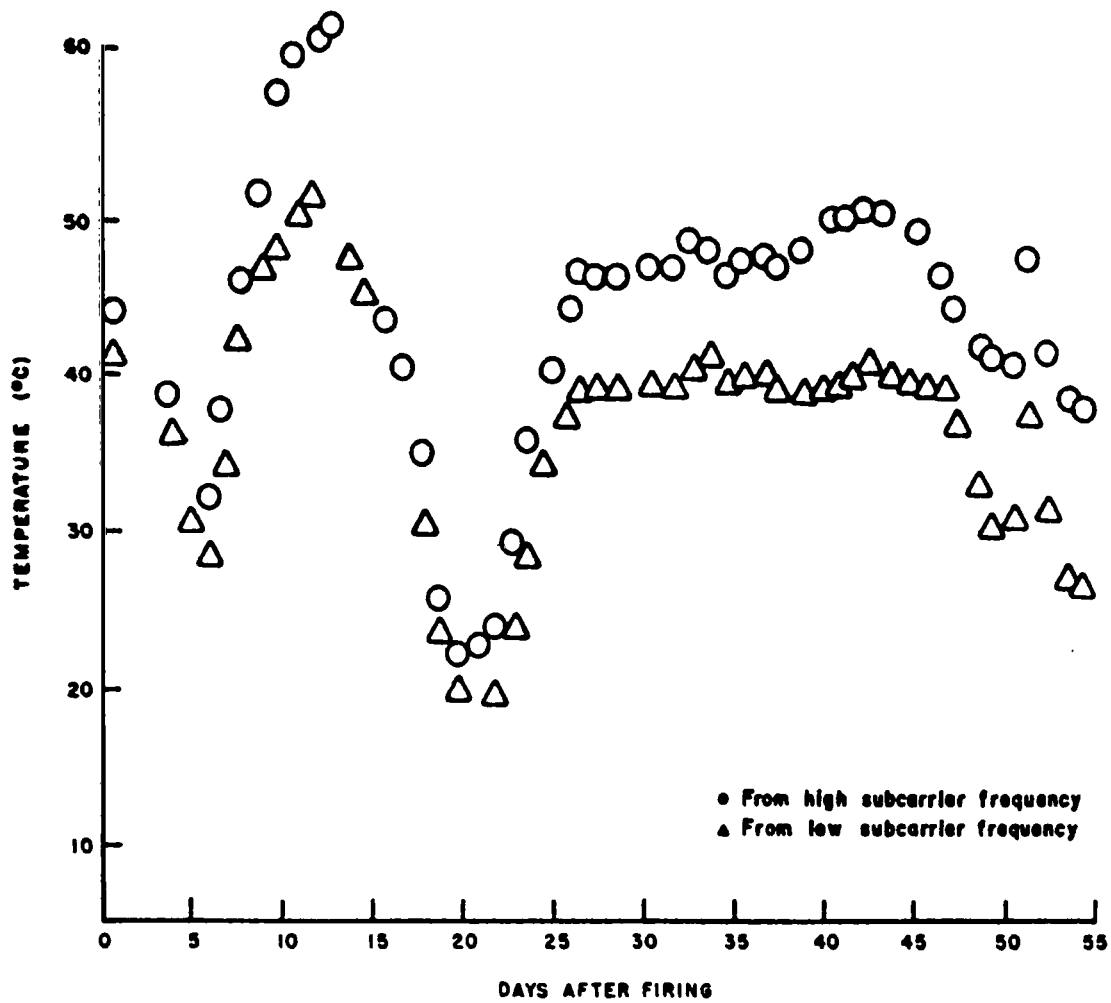


FIGURE 5. EXPLORER IV TEMPERATURES MEASURED DURING TRANSMITTER LIFETIME FROM THE CHANNEL 3 SUBCARRIER FREQUENCY

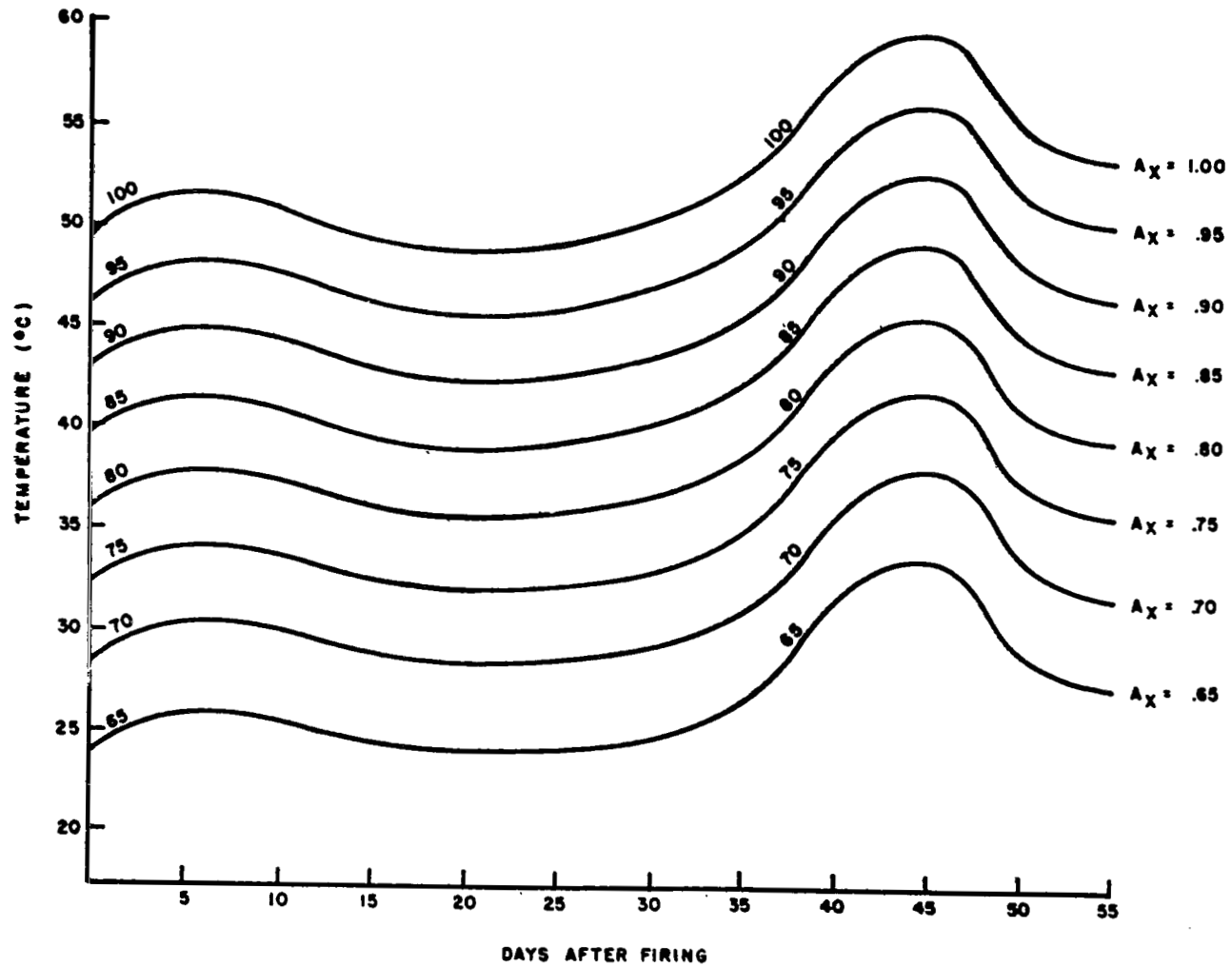


FIGURE 6. CALCULATED TEMPERATURES FOR EXPLORER IV FOR VARIOUS FRACTIONS OF THE LONGITUDINAL AREA PRESENTED TO THE SUN

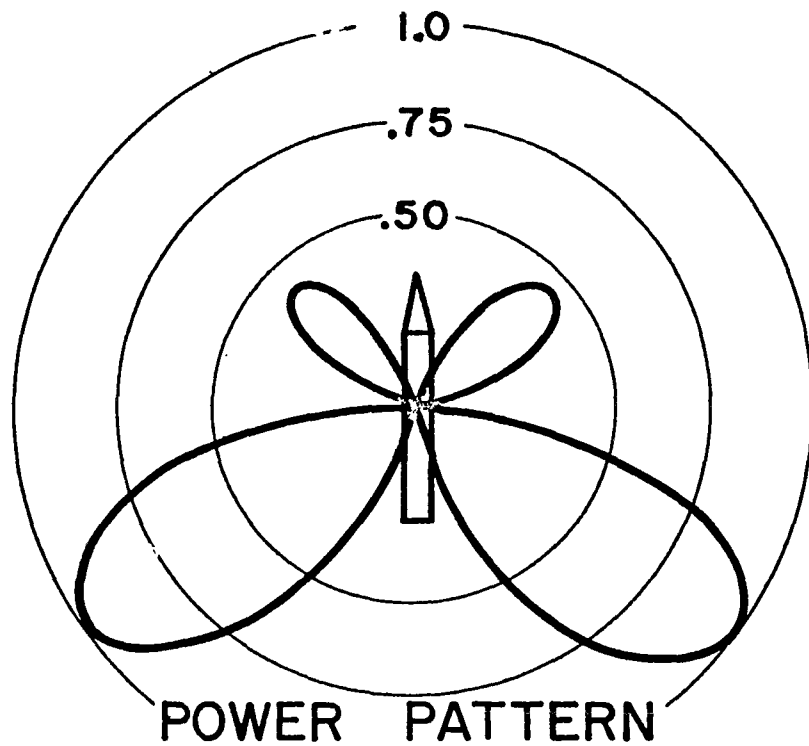
SECTION II. DETERMINATION OF THE TUMBLE AXIS

A. DISCUSSION OF THE TUMBLE AXIS DETERMINATION

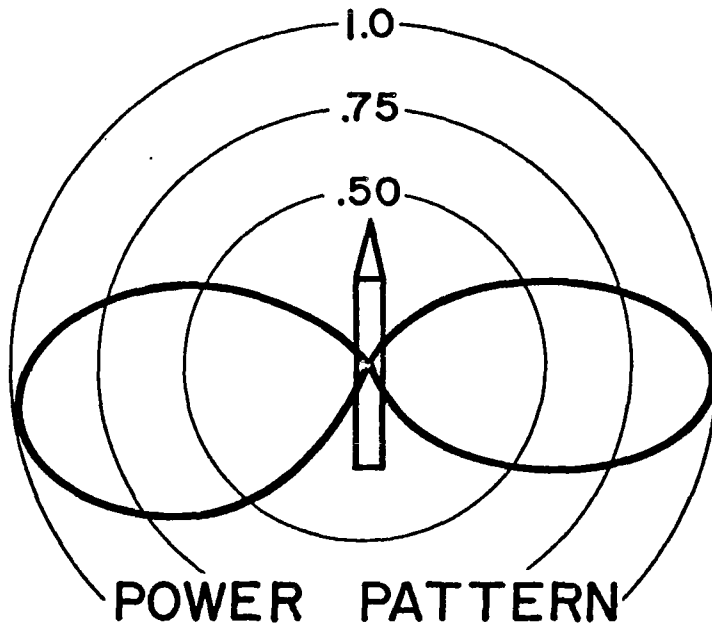
As previously pointed out, the orientation of the tumble axis must first be determined in order to obtain the counter orientation. This becomes somewhat problematical since the satellite was not provided with any onboard sensors for this purpose. However, examination of the satellite antenna radiation patterns suggests a method whereby the look angle, or the angle that the line of sight from the tracking station to the satellite makes with tumble axis, may be inferred from the recorded signal strength variations [Ref. 38]. Figure 7 shows these radiation patterns for the 108 mc/sec and 108.03 mc/sec transmitters. It may be seen that the 108 mc/sec antenna, being an asymmetrical dipole, has a minor lobe on either side of the nose of the satellite whereas the 108.03 mc/sec antenna exhibits a characteristic dipole pattern. In either case the radiation is linearly polarized in a plane containing the symmetry axis.

If the satellite is viewed along the tumble axis with a linearly polarized receiving antenna, fading will be observed at twice the tumble frequency because of the rotating plane of polarization of the emitted radiation. The plane of polarization is also rotated by the Faraday effect resulting from magneto-ionic splitting [Refs. 39, 40] as the signal traverses the ionosphere. The rotation rate of the latter effect, which is due to the changing integrated electron density along the path of propagation as the satellite moves relative to the tracking station, is slow compared to the tumble rate for frequencies of 108 mc/sec. Therefore, it does not materially change the observed patterns of signal strength variations. Thus, for the case where the look angle Ψ is small, that is, when the satellite is viewed almost along the tumble axis, the signal strength variations are essentially the same for both transmitters.

If the satellite is viewed in the plane of tumble, fades will occur in the 108.03 mc/sec signal strength patterns at twice the tumble frequency due to the nulls in the antenna radiation pattern. These nulls are indistinguishable from those caused by polarization fading in the case of small Ψ ; consequently, the 108.03 mc/sec signal strength variations do not provide usable information if a linearly polarized tracking antenna is used. However, when viewing in the tumble plane, the small lobes on either side of the nose are apparent in the 108 mc/sec signal strength patterns. This distinguishing feature then enables one to determine whether the look angle Ψ is large or small. As it turned out, most of the signal strength recordings taken by the Huntsville Tracking Station contained the small lobes in the 108 mc/sec pattern. On two days, August 12 and 18, passes were observed in which the small lobes were absent for an interval of time during the pass. A simulation of the observed signal strength variations was performed on an analogue computer in which it was shown that the small lobes would be visible in the signal strength variations unless Ψ was less than about 20 degrees.



108.00 mc



108.03 mc

FIGURE 7. EXPLORER IV ANTENNA RADIATION PATTERNS

The line of sight vector was computed at the times where the small lobes were absent on the August 12 and 18 passes. This computation was done by subtracting the vector from the center of the earth to the tracking station from the radius vector to the satellite. The former is known from the geodetic coordinates of the station. The latter is found from the geodetic position of the satellite which is listed in one-minute intervals in the Smithsonian Astrophysical Observatory ephemeris [Ref. 41]. The resultant line of sight vector was then transformed into an earth-centered, right-handed, space orientation-fixed coordinate system in which the x-axis is in the direction of the vernal equinox and the z-axis is along the north celestial pole. To facilitate the plotting of this vector, which was normalized and designated as \vec{U} , it is desirable to express it in terms of two position angles: right ascension and declination. Since the satellite is tumbling essentially in a plane, one should expect to observe the same signal strength variations on either side of the plane. Hence, the same pattern should be observed when looking along \vec{U} as when looking along $-\vec{U}$. Therefore, the \vec{U} was plotted as well as $-\vec{U}$ for each pass. Figure 8 is such a plot of the sight vector for two passes on August 12. The single lines indicate the orientations of the sight vector when the small lobes were visible on the signal strength recordings - hence $\Psi > 20$ degrees. The double lines indicate the orientations of the sight vector when these lobes were absent or when $\Psi < 20$ degrees. The dashed line around the region where Ψ was observed to be less than 20 degrees represents the intersection of a cone whose half angle is 20 degrees and the celestial sphere. This fit is determined graphically and the axis of the cone is assumed to be parallel to the tumble axis. At this point, there is no way of determining the sense of tumble; hence, the angular momentum vector of the satellite may either be parallel or anti-parallel to the cone axis. Figure 9 is a similar determination of the tumble axis obtained from two passes on August 18.

Unfortunately, many passes recorded by the Huntsville Tracking Station prior to August 18 did not contain useable signal strength recordings. Also, the condition that Ψ be less than 20 degrees to provide useful orientation data was not frequently met. It became apparent that if a history of the tumble axis orientation over the satellite transmitter lifetime was to be determined, an alternate method must be found. On August 18, the Huntsville Tracking Station altered their receiving antenna system. Instead of using a single dipole array, an attempt to obtain polarization diversity by adding another dipole array with crossed polarization was made. The two antenna arrays were mounted on separate pedestals, being separated by about 50 meters. Their outputs were added a "T" junction and then detected by a single Hallamore receiver. As the satellite moved overhead, the path length to the two antennas changed, thus altering the phase angle between the two antenna outputs. This produced an interferometer effect that altered the effective polarization of the receiving antenna. For example, if the two output voltages are in phase, the array is effectively plane polarized at 45 degrees to each element. As the phase angle becomes 90 degrees, the array becomes circularly polarized. The location of the antennas was such that the polarization change was usually slow compared to the tumble rate so that several tumble cycles could be observed at more or less constant polarization.

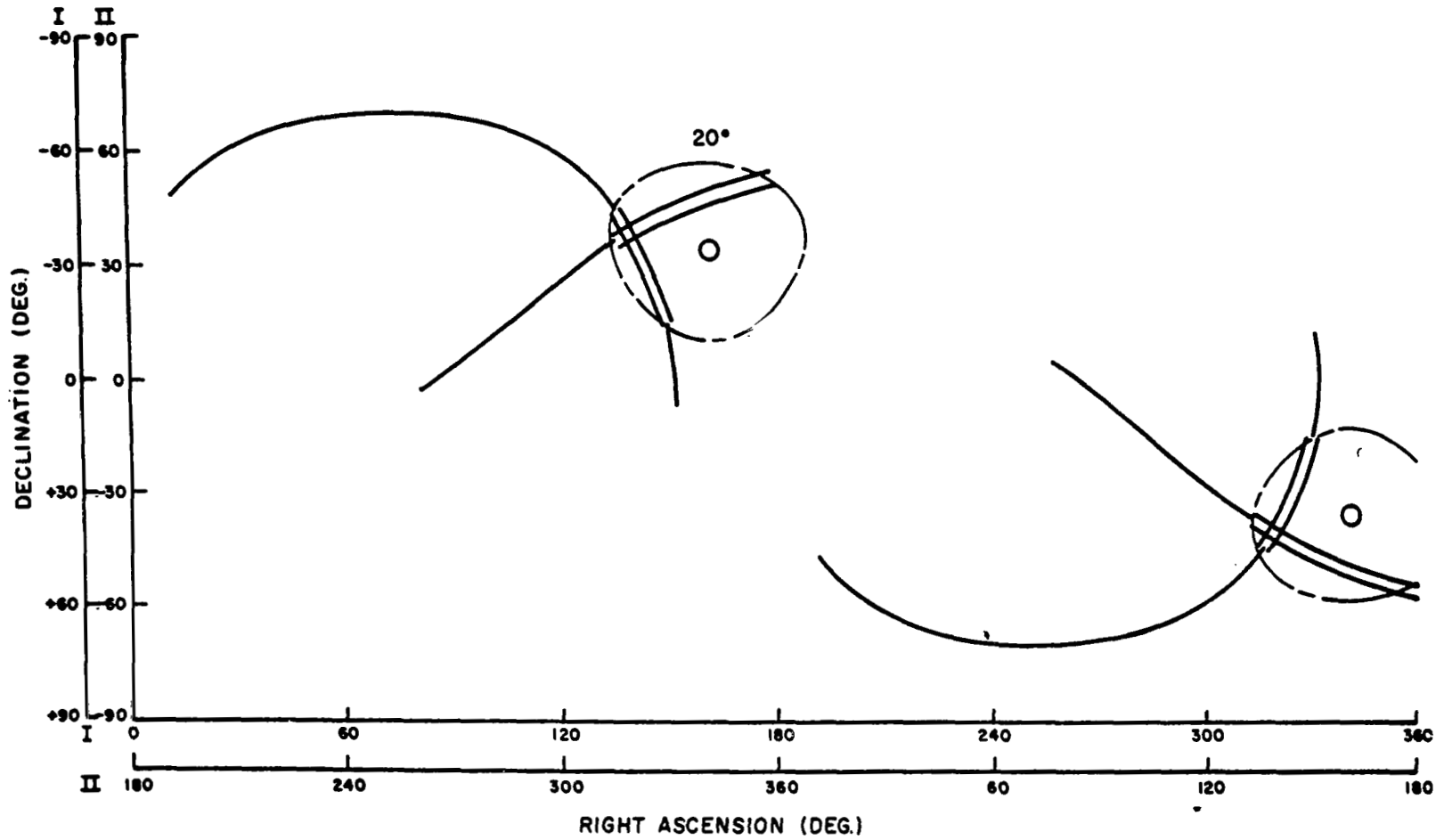


FIGURE 8. RIGHT ASCENSION AND DECLINATION OF SIGHT VECTOR FOR PASSES DURING AUGUST 12, 1958

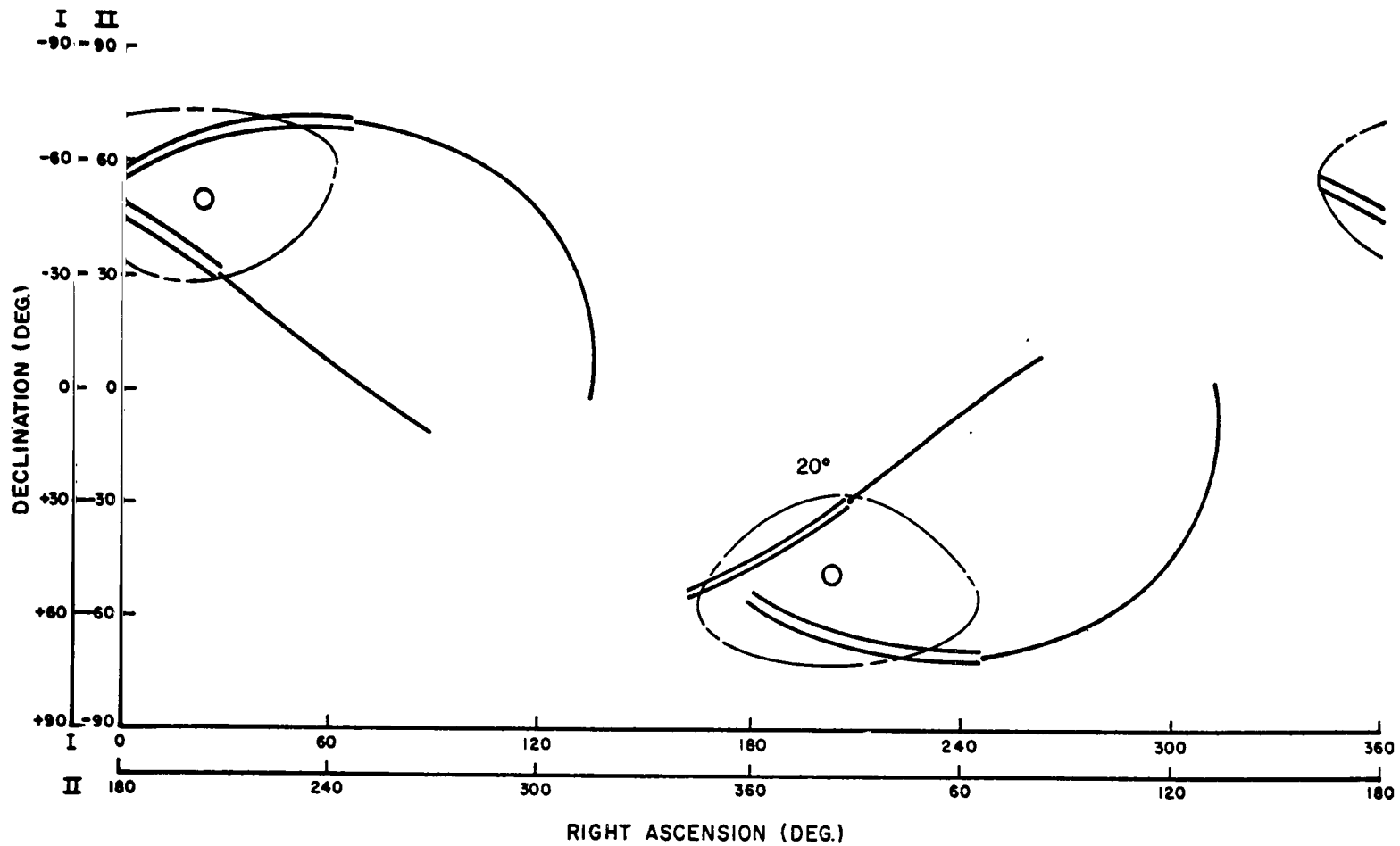


FIGURE 9. RIGHT ASCENSION AND DECLINATION OF THE SIGHT VECTOR FOR AUGUST 18, 1958

This technique allowed the use of 108.03 mc/sec signal strength patterns. The times when the antenna array was circularly polarized could be obtained by observing when the fades were less severe. At these times, the amplitude of the fades allowed an estimate of the look angle. Lack of calibration on the recorded signal strength records precluded an accurate measurement of the look angle; but a crude estimate could be made on the basis of comparison of the fading amplitude observed during the circularly polarized portion with the more severe fades observed when the antenna was linearly polarized. If the signal strength exhibited periods where little or no fading was evident, such as shown in Figure 10, the look angle Ψ was estimated to be less than 30 degrees. If the fading was discernible, but still much less than the severe fades as in Figure 11, Ψ was estimated to be between 30 degrees and 45 degrees. If the observed signal was a mixture of antenna radiation pattern fades and polarization fades as shown in Figure 12, Ψ was estimated to be from 45 degrees to 60 degrees. If the pattern was predominately antenna radiation pattern fades, lessened only slightly as the polarization changes, Ψ was estimated to be 60 degrees to 75 degrees. Figure 13 is an example of this pattern. If Ψ was between 75 degrees and 90 degrees, severe fades due to the radiation nulls along the nose and tail were observed regardless of the polarization of the receiving antenna. This is shown in Figure 14.

For days when a sufficient number of passes were available, the right ascension and declination of the sight vector at various times during the passes were plotted in the manner described previously. The type of signal strength variation noted is indicated by shading. A set of transparent overlays were prepared showing the intersections on the celestial sphere of a family of cones of various half angles about an axis having a particular declination. These overlays were used to determine graphically the position of the tumble axis that best satisfied the observed signal strength patterns. Figures 15 to 20 show this determination for various days in August and September. The right ascension of the tumble axis can be fairly well determined by making use of the 75 degrees to 90 degrees patterns in the signal strength which appear to be fairly reliable. The declination is probably determined with less certainty since it is generally near the equator and not well bracketed by the 75 degrees to 90 degrees patterns.

An effort was made to obtain more information on the orientation of the tumble axis by examining data from other tracking stations. Unfortunately, little usable data was found since many stations did not record signal strength or did not use antenna systems that facilitated analysis of the signal strength variations in terms of look angle. Some useful data was obtained from the station operated by the Stanford Research Institute located at Johnston Island. This station used a steerable, circularly polarized, crossed Yagi antenna; however, they did record signal strength. It was noted in the 108.03 mc/sec telemetry records taken by this station that were intervals where the count rate data was uninterrupted by fades. At other times, the telemetry was interrupted every 3.5 second by fading that was presumably caused by the signal strength dropping below the receiver sensitivity. When Ψ is small the signal strength

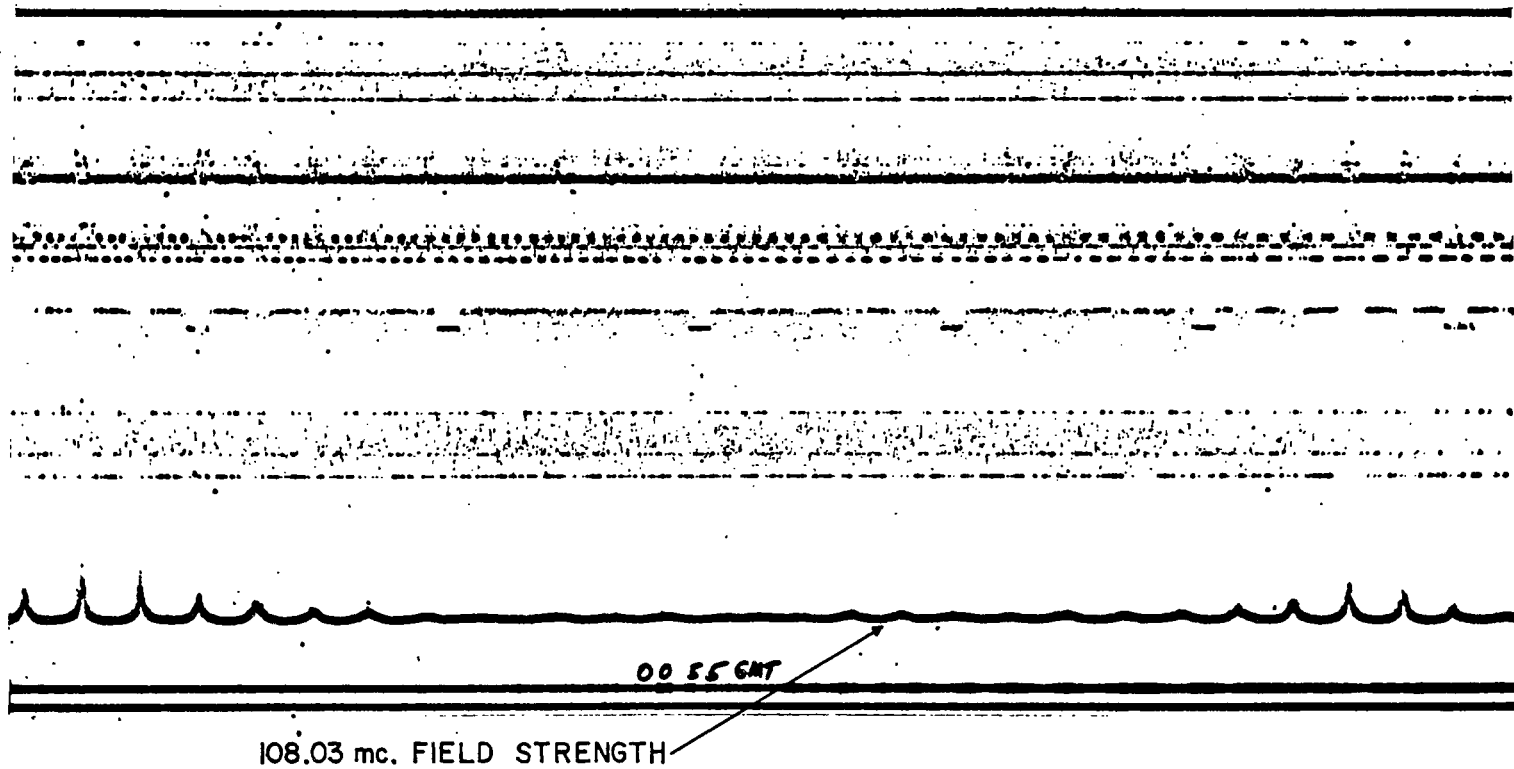


FIGURE 10. TELEMETRY SAMPLE SHOWING THE 108.03 mc/sec SIGNAL STRENGTH FOR $\psi < 30^\circ$

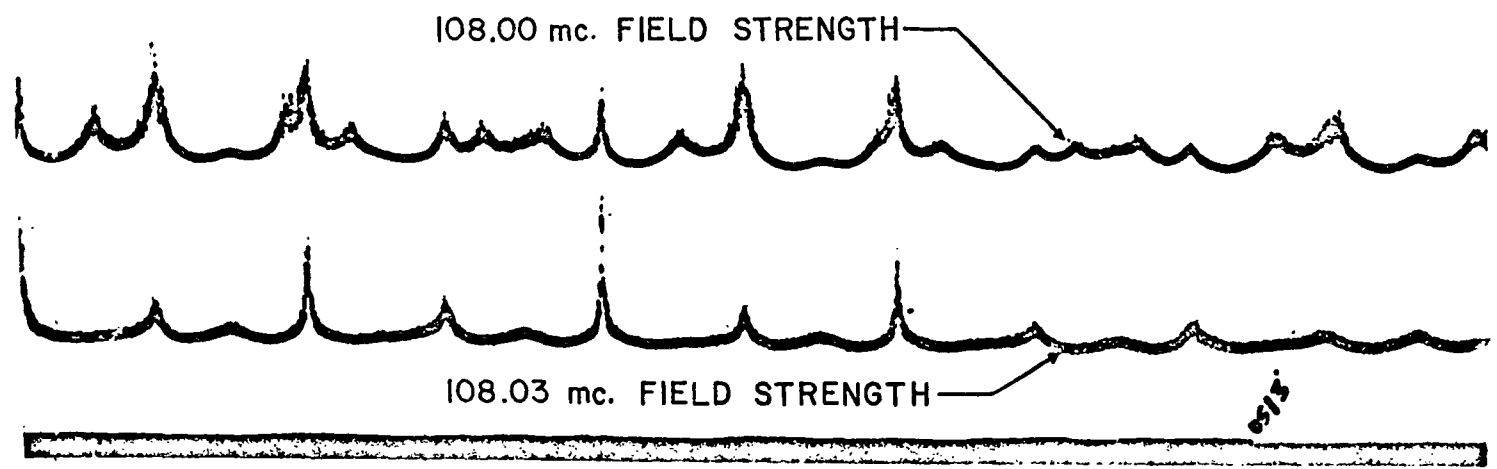


FIGURE 11. TELEMETRY SAMPLE ILLUSTRATING THE SIGNAL STRENGTH VARIATIONS FOR THE CASE OF $30^\circ < \Psi < 45^\circ$

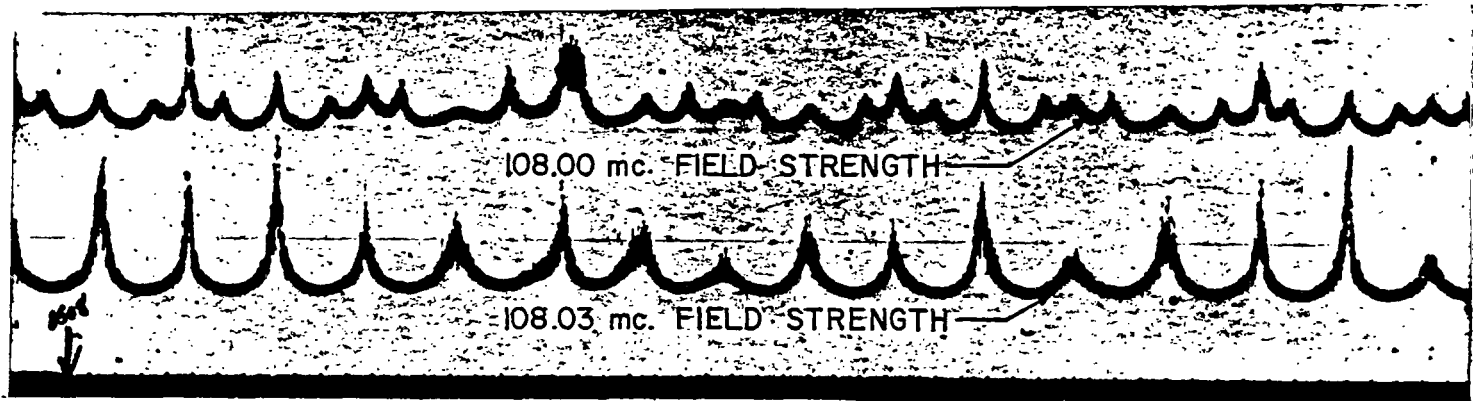


FIGURE 12. TELEMETRY SAMPLE ILLUSTRATING THE SIGNAL STRENGTH VARIATIONS FOR THE CASE OF $45^\circ < \Psi < 60^\circ$

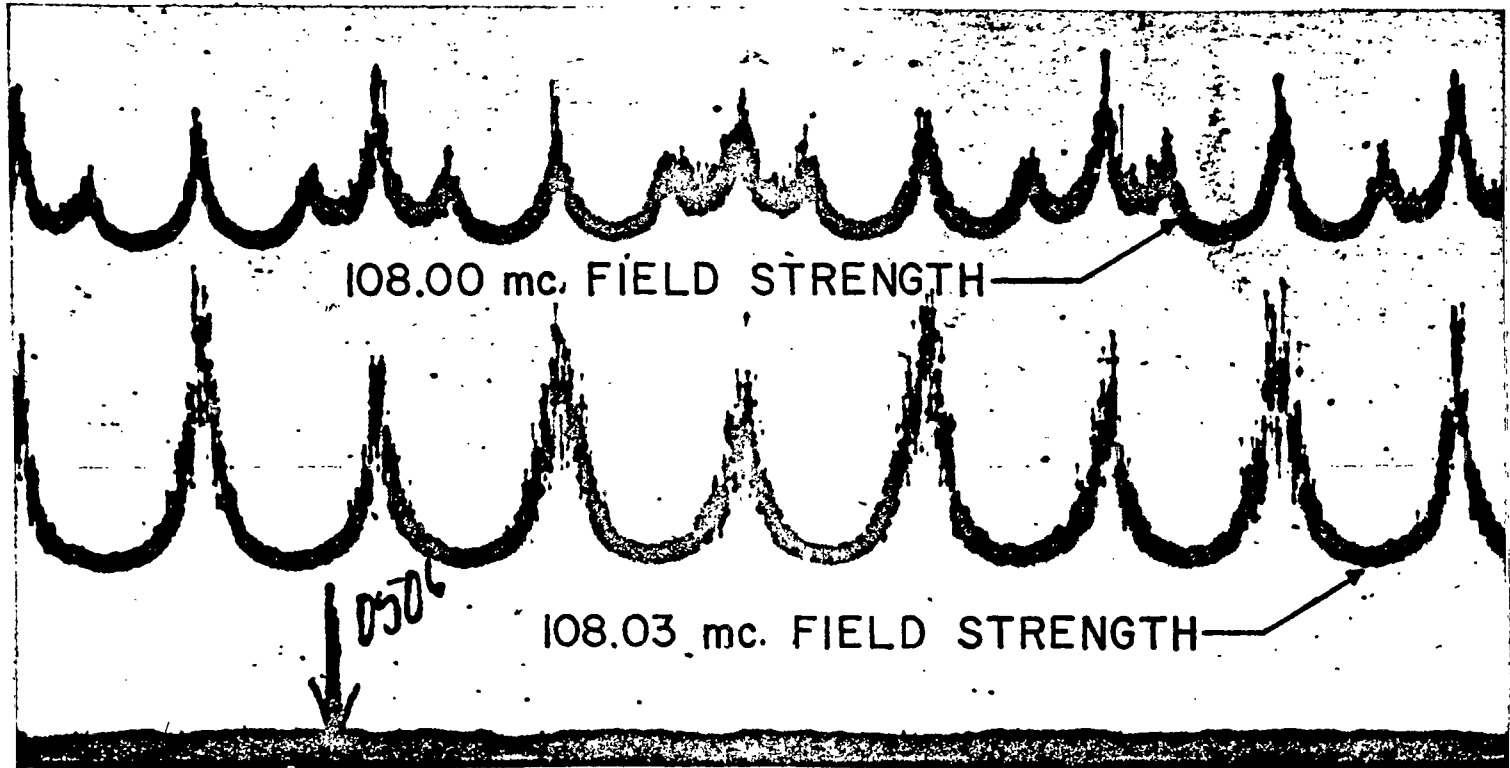


FIGURE 13. TELEMETRY SAMPLE ILLUSTRATING THE SIGNAL STRENGTH FOR THE CASE OF $60^\circ < \Psi < 75^\circ$

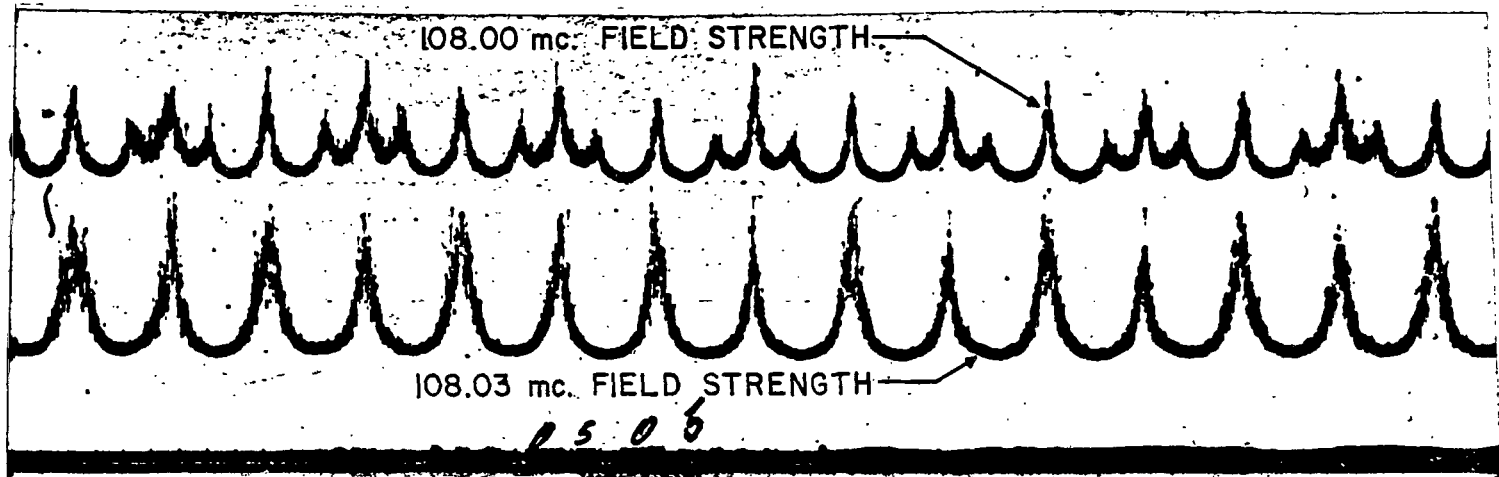


FIGURE 14. TELEMETRY SAMPLE ILLUSTRATING THE SIGNAL STRENGTH VARIATION FOR THE CASE OF $75^\circ < \psi < 90^\circ$

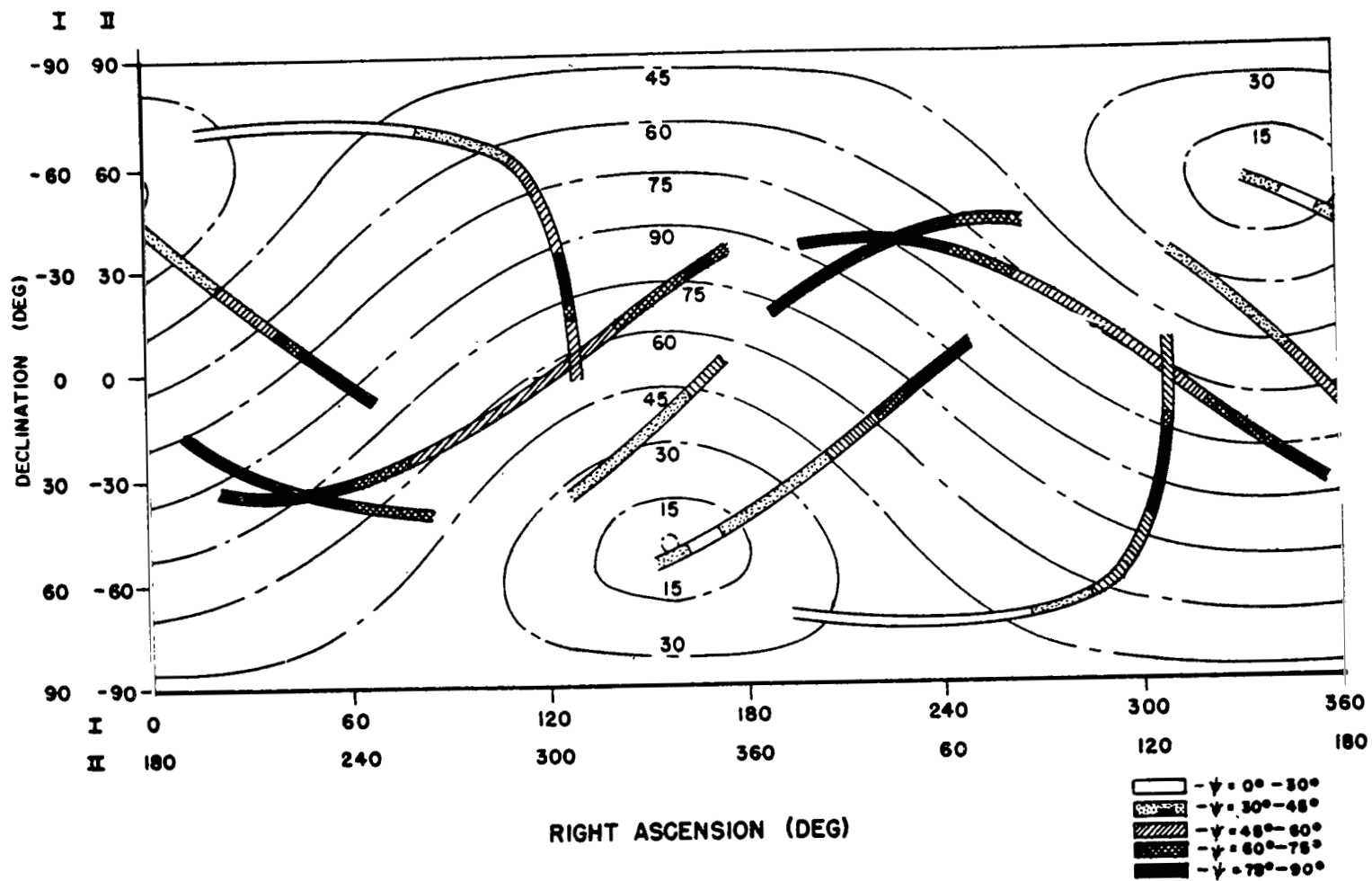


FIGURE 15. RIGHT ASCENSION AND DECLINATION OF THE SIGHT VECTOR FOR PASSES DURING AUGUST 20, 1958

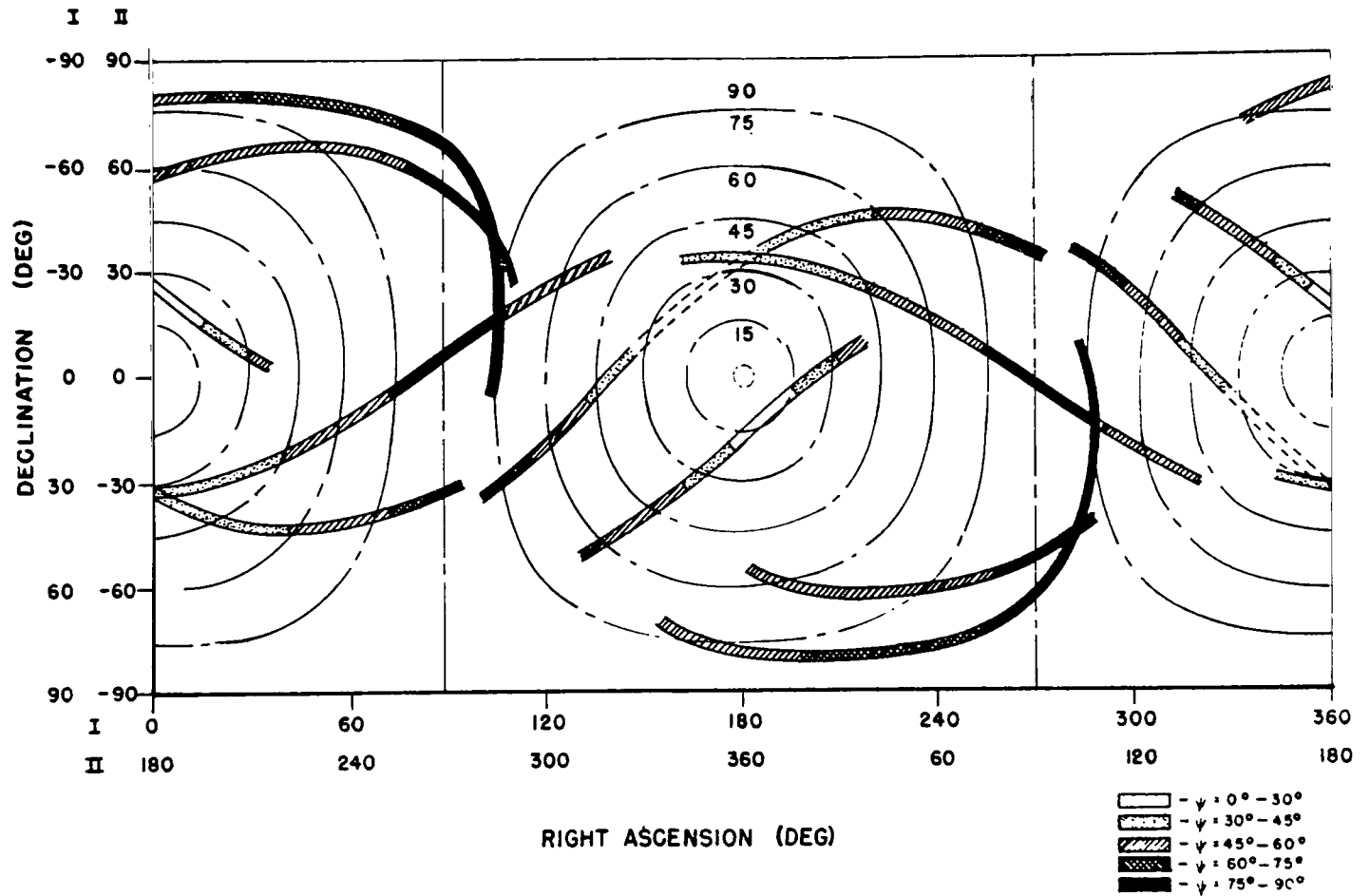


FIGURE 16. RIGHT ASCENSION AND DECLINATION OF SIGHT VECTOR FOR PASSES DURING AUGUST 27, 1958

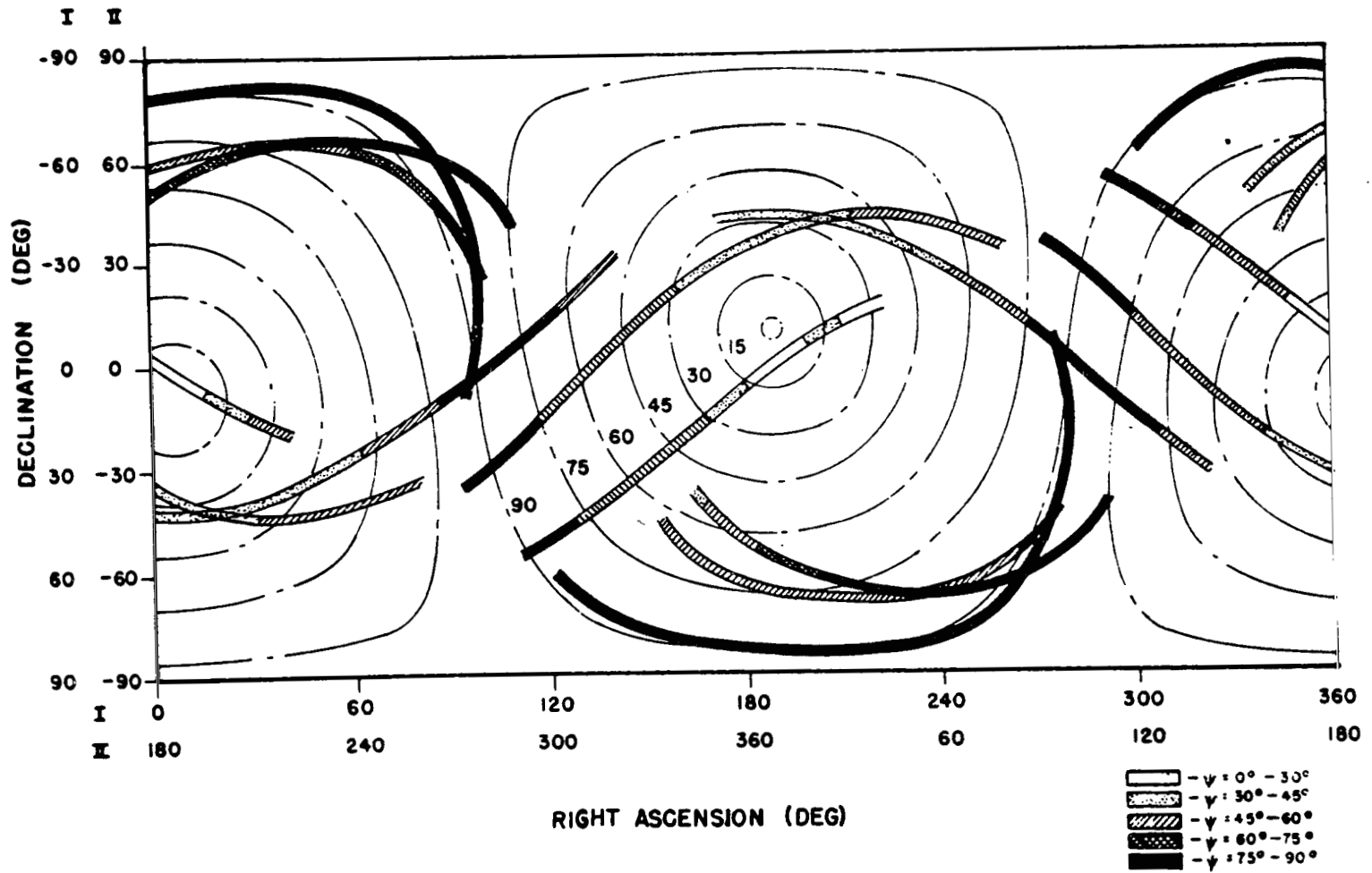


FIGURE 17. RIGHT ASCENSION AND DECLINATION OF SIGHT VECTOR FOR PASSES DURING AUGUST 30, 1958

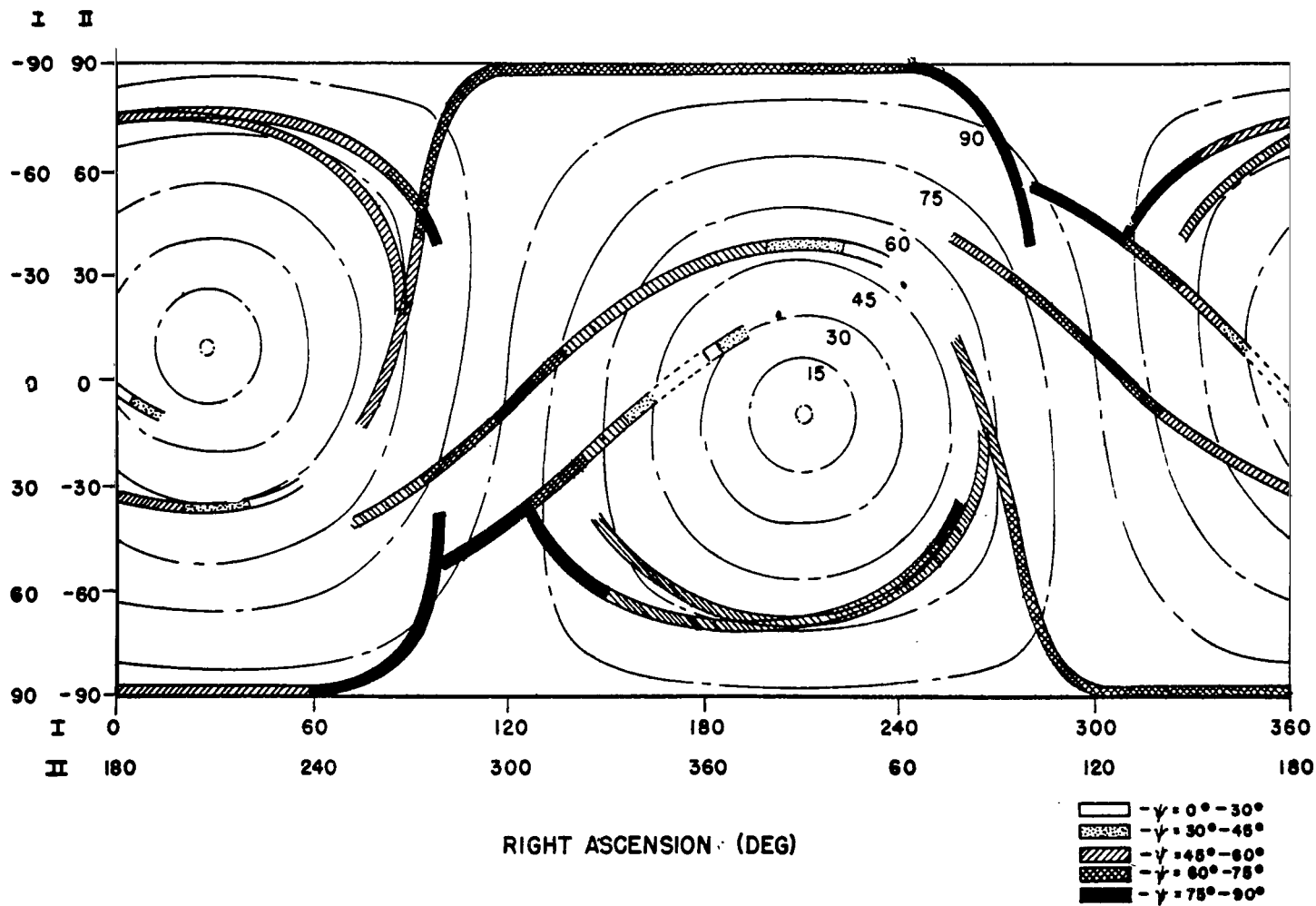


FIGURE 18. RIGHT ASCENSION AND DECLINATION OF THE SIGHT VECTOR FOR PASSES DURING SEPTEMBER 3, 1958

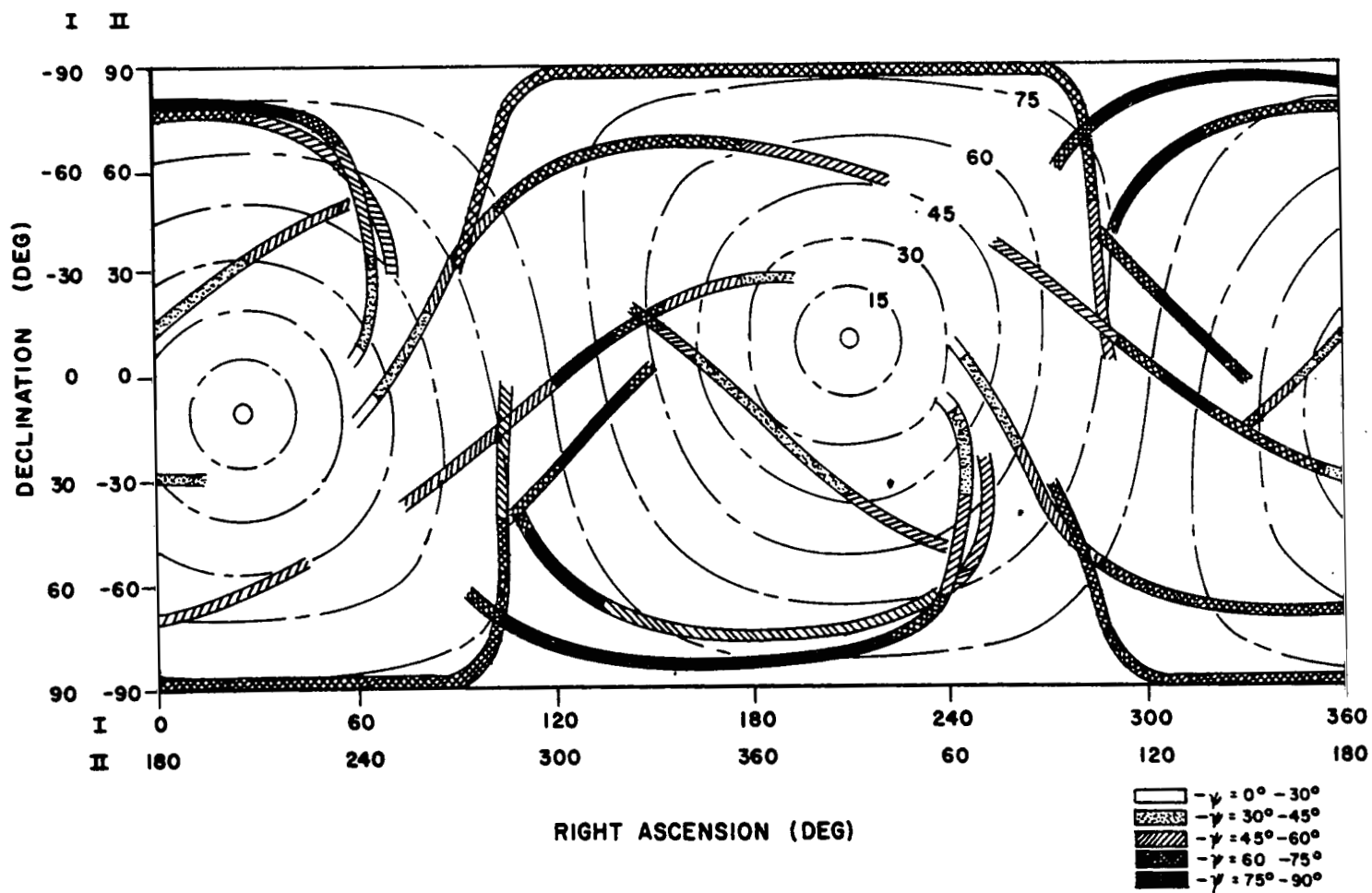


FIGURE 19. RIGHT ASCENSION AND DECLINATION OF THE SIGHT VECTOR FOR PASSES DURING SEPTEMBER 10, 1958

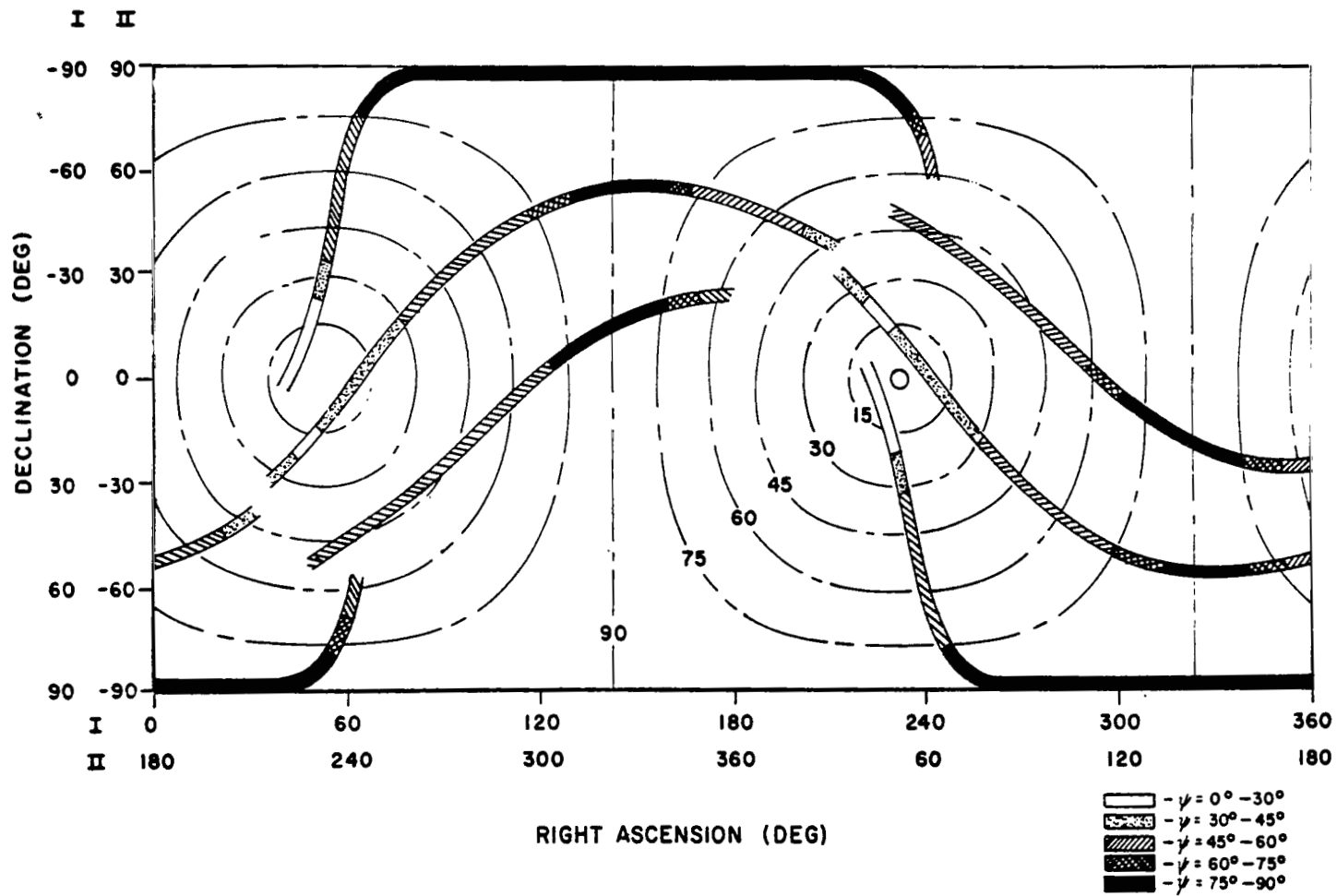


FIGURE 20. RIGHT ASCENSION AND DECLINATION OF THE SIGHT VECTOR FOR PASSES DURING SEPTEMBER 14, 1958

variations are small, and since the antenna is not affected by polarization of the incident radiation, one would expect uninterrupted data. When Ψ is large, fades would be expected because of the observance of the radiation nulls along the satellite nose and tail. It is not known what values of Ψ will just begin to produce fades since this depends on the receiver sensitivity, the distance from the satellite to the station, the power radiated by the satellite and any attenuation suffered along the path of propagation. The orientation of the sight vector was plotted at the times the signal was uninterrupted resulting in Figures 21 and 22. The dashed line indicates a cone of 45 degrees half-angle which appears to define the region on the celestial sphere in which the signal strength does not drop below the receiver sensitivity. The axis of this cone is again assumed to be parallel to the tumble axis.

The methods used for determining the tumble axis are admittedly crude, since the look angles could only be estimated. Graphical fitting was used primarily for expediency. While a more elegant numerical method could have been attempted, it was not felt justifiable in light of the crudeness of the data. Furthermore, it was necessary to use several passes during the same day to define the tumble axis sufficiently. Since the tumble axis may have shifted by as much as 10 degrees during this time, the best that can be hoped for is some mean location that may be considered effective for that day.

To obtain an analytical description of the excursions of the tumble axis, the right ascensions and declinations obtained by this analysis were plotted as a function of days after launch. A polynomial description using two 9th-degree polynomials was attempted. Figure 23 shows the result of attempting to fit polynomials to the right ascension and declination of the tumble axis. No data is available from launch until August 9; hence, the polynomials are not defined except from August 9 to September 11. The polynomial description for declination from September 3 to September 9 does not appear to fit the observed data very well, but because of the previously mentioned uncertainties in determining declinations near the equator this discrepancy will be disregarded.

B. CONFIRMATION OF THE TUMBLE AXIS DETERMINATION

Having obtained polynomials that describe the motion of the tumble axis, the angle made by the position vector of the sun with the tumble axis may readily be found. From this angle the average insolated area during a tumble cycle may be calculated. Then using the curves of predicted interior temperature for various insolated areas prepared by Snoddy (Fig. 6), the temperature may be found as a function of time. This result is plotted over the observed temperature in Figure 24. The dotted line in the plot represents the temperature predicted if the tumble axis had retained its initial spatial orientation. There is a discrepancy in the temperature obtained from the high frequency state of the subcarrier oscillator as compared to that obtained from the low frequency state which is probably due to some frequency drift which occurred after the calibration was made. This discrepancy appears to be uniform throughout the

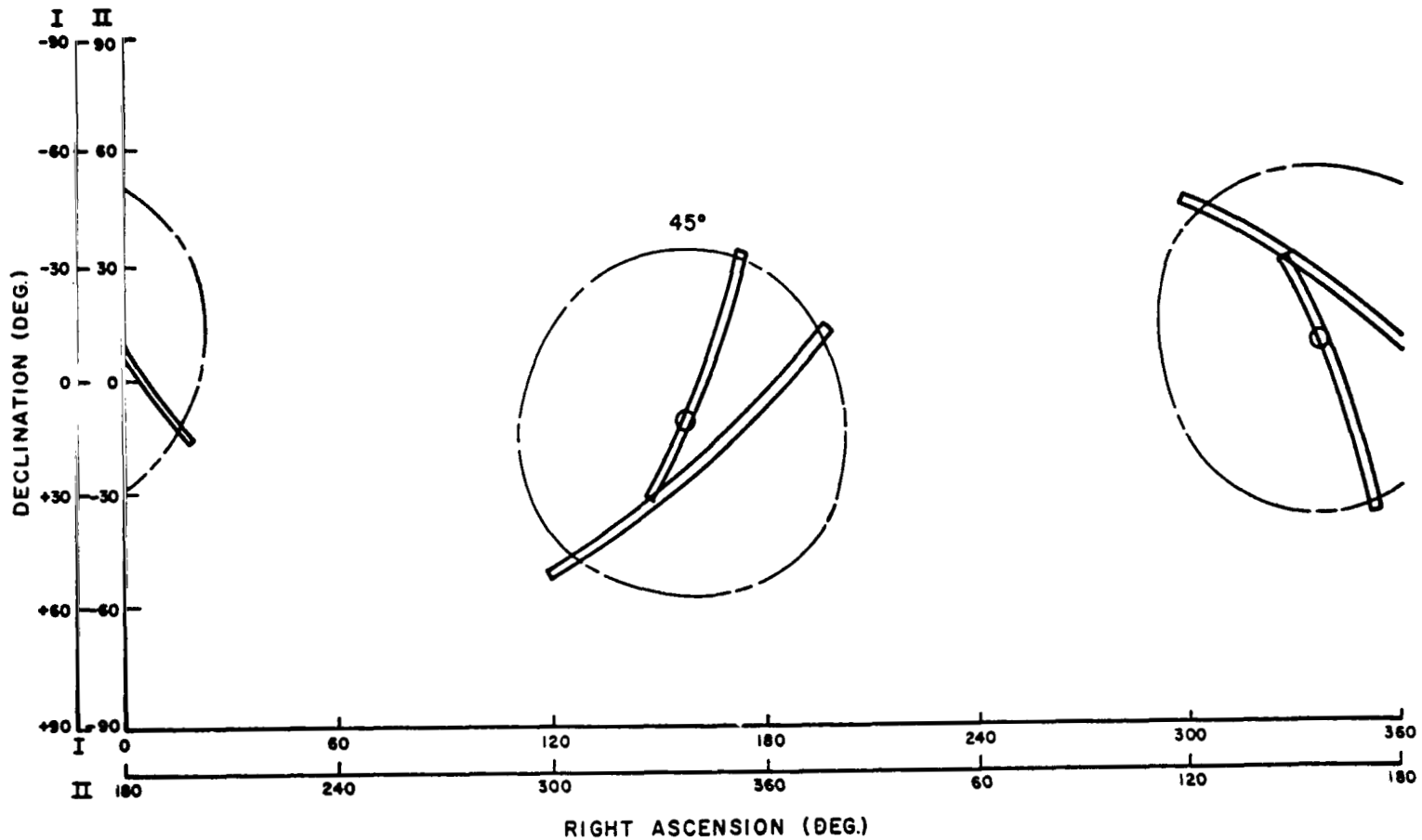


FIGURE 21. RIGHT ASCENSION AND DECLINATION OF THE SIGHT VECTOR FOR AUGUST 9, 1958 AT TIMES WHEN FADING WAS NOT OBSERVED IN THE TELEMETRY RECEIVED BY THE JOHNSTON ISLAND STATION

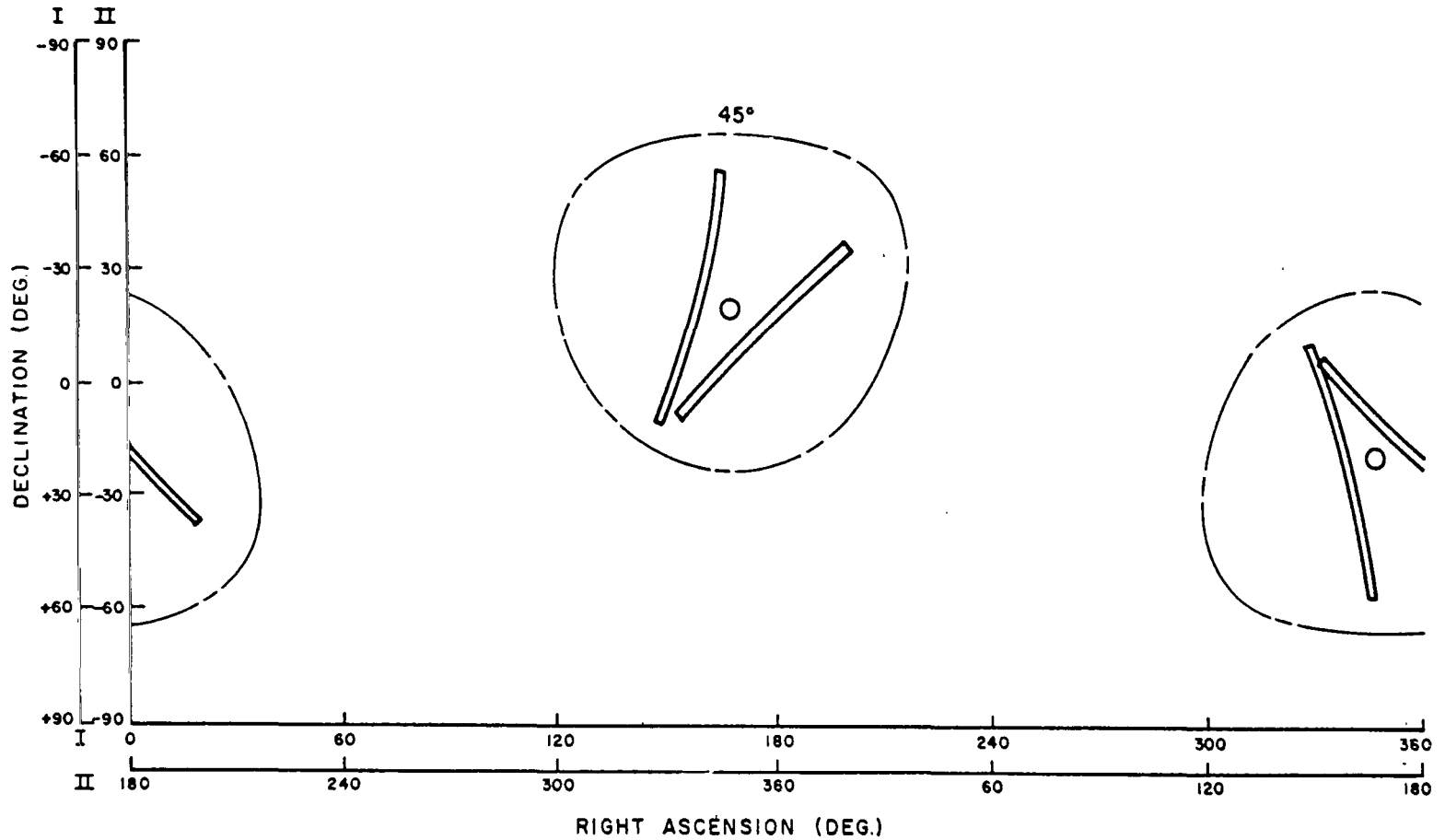


FIGURE 22. RIGHT ASCENSION AND DECLINATION OF SIGHT VECTOR AT TIMES FADING WAS ABSENT FROM JOHNSTON ISLAND TELEMTRY ON AUGUST 11, 1958.

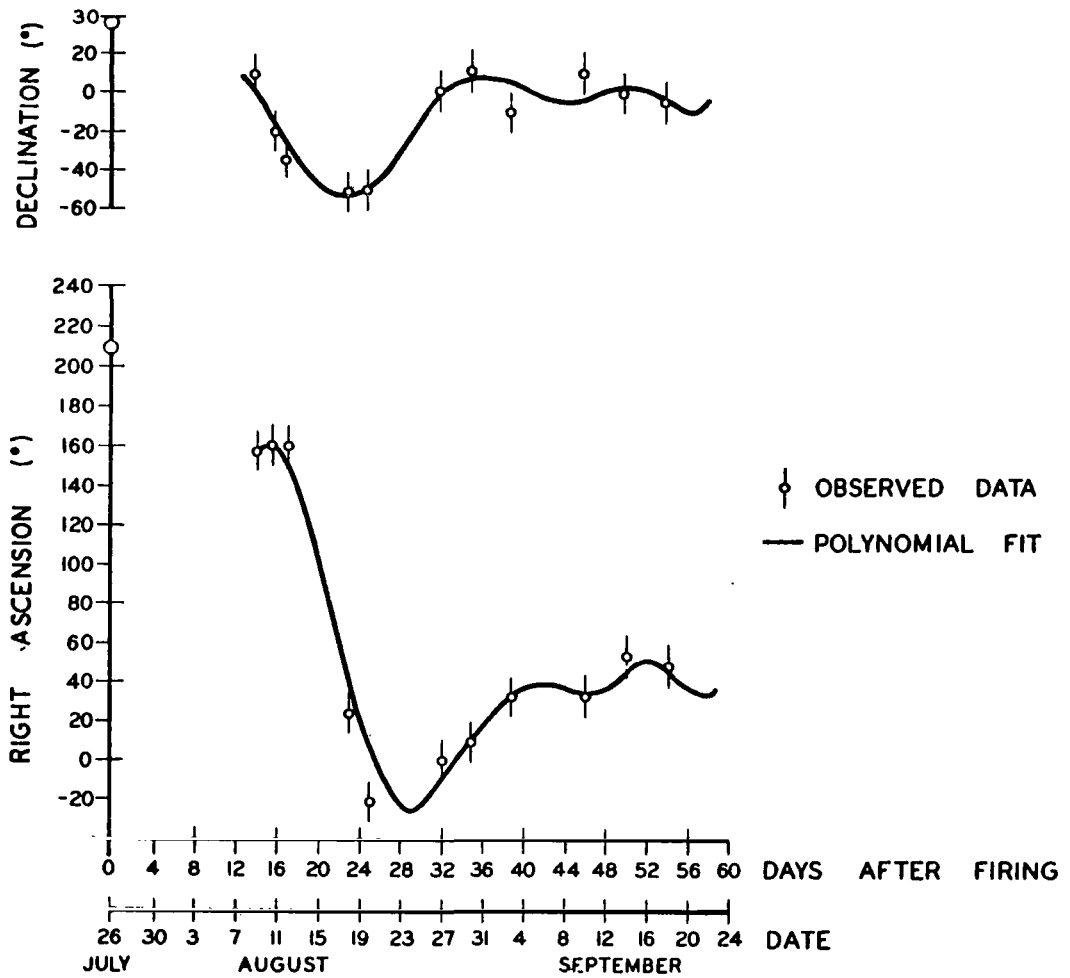


FIGURE 23. POLYNOMIAL DESCRIPTION OF THE RIGHT ASCENSION AND DECLINATION OF THE ANGULAR MOMENTUM VECTOR

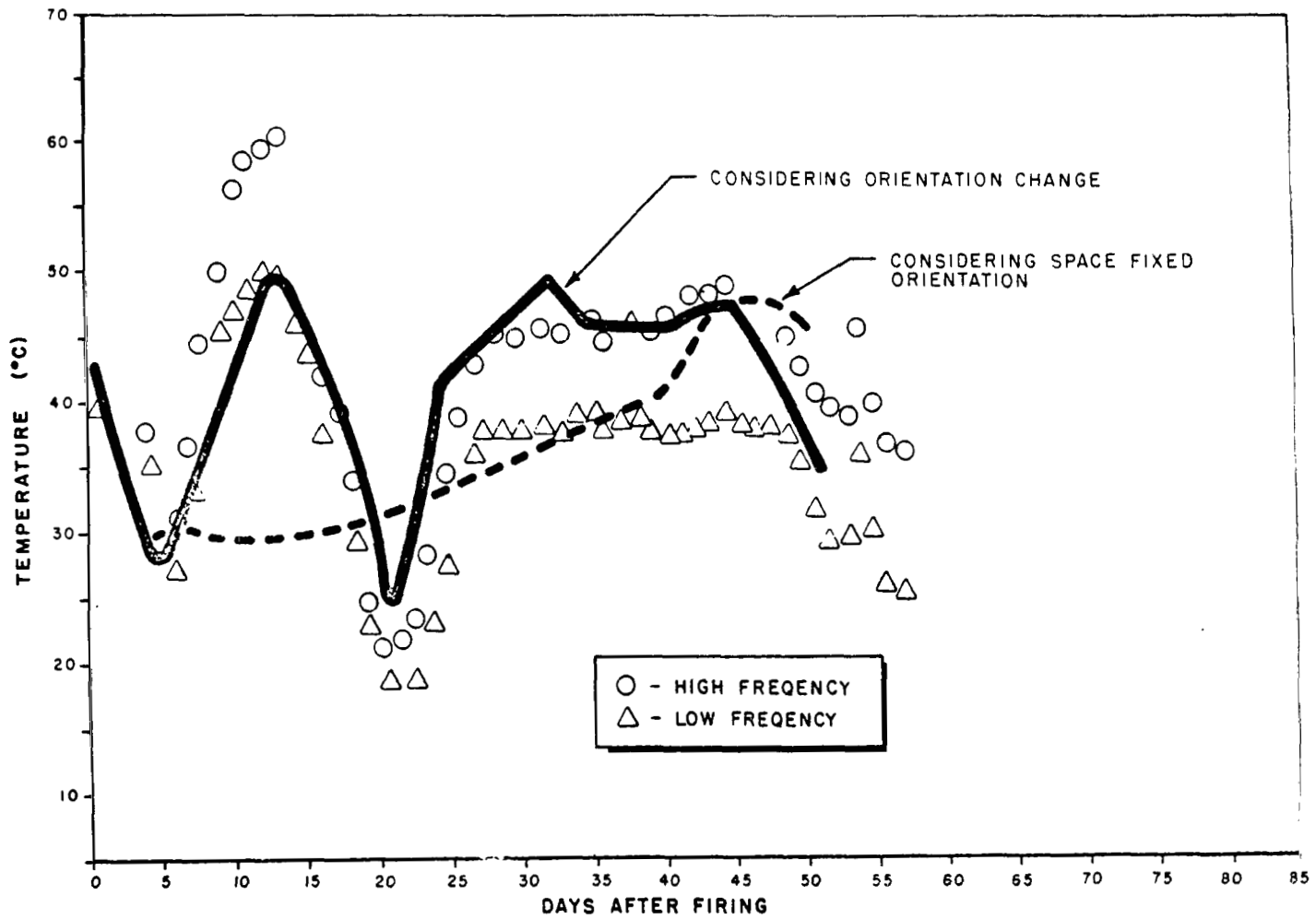


FIGURE 24. COMPARISON OF CALCULATED TEMPERATURES WITH OBSERVED TEMPERATURES

transmitter lifetime. Although the actual temperature may not be known exactly, the observed temperature fluctuations appear to be consistent with those predicted from the determination of the tumble axis.

The change in orientation of the plane of tumble should also result in drag variations because of a change in average frontal area presented to the atmosphere at perigee. Such fluctuations were observed by Lautman at the Smithsonian Astrophysical Observatory [Refs. 42, 43]. Figure 25 shows the period loss per revolution due to drag forces. Using the polynomials for the tumble axis description, the angle that the tumble axis makes with the perigee velocity vector was found and the resultant average drag area was calculated. Figure 26 shows the computed average frontal area as a function of time. It may be seen that, in general, the loss of period is greatest when the drag area is large. Of course there are other factors that influence drag losses, such as a variation of atmospheric density which appears to be related to solar activity [Ref. 44].

In a study of the effect of the tumble axis orientation relative to magnetic field on counting rate observed by the directional radiation detectors on Explorer IV, Shelton points out that certain counting rate patterns should be characteristic of certain values of the dot product of the tumble axis \vec{L} and the magnetic field direction \vec{B} [Refs. 45, 46]. The polynomial for L was incorporated in the program [Ref. 47] for computing the satellite position and the local geomagnetic field components using the Finch and Leaton [Ref. 48] 48 term expansion. The result of this program was a listing of the dot product of \vec{L} and \vec{B} at one-minute intervals from August 9 through the transmitter lifetime. Using these results, Fields was able to match the observed counting rate patterns with those predicted by the computed \vec{L} and \vec{B} on several occasions [Ref. 49].

It is difficult to say how accurate the previous tumble axis determination actually is, although the success in explaining the observed temperature and the drag variations is encouraging. It is felt that the determination is generally good to about ± 10 degrees in angular position with possibly somewhat higher uncertainty in declination during the times when the tumble axis lies near the equator. It will be shown later that uncertainties of this magnitude do not seriously detract from the accuracy of obtaining count rate as a function of the angle the counter axis makes with the magnetic field lines.

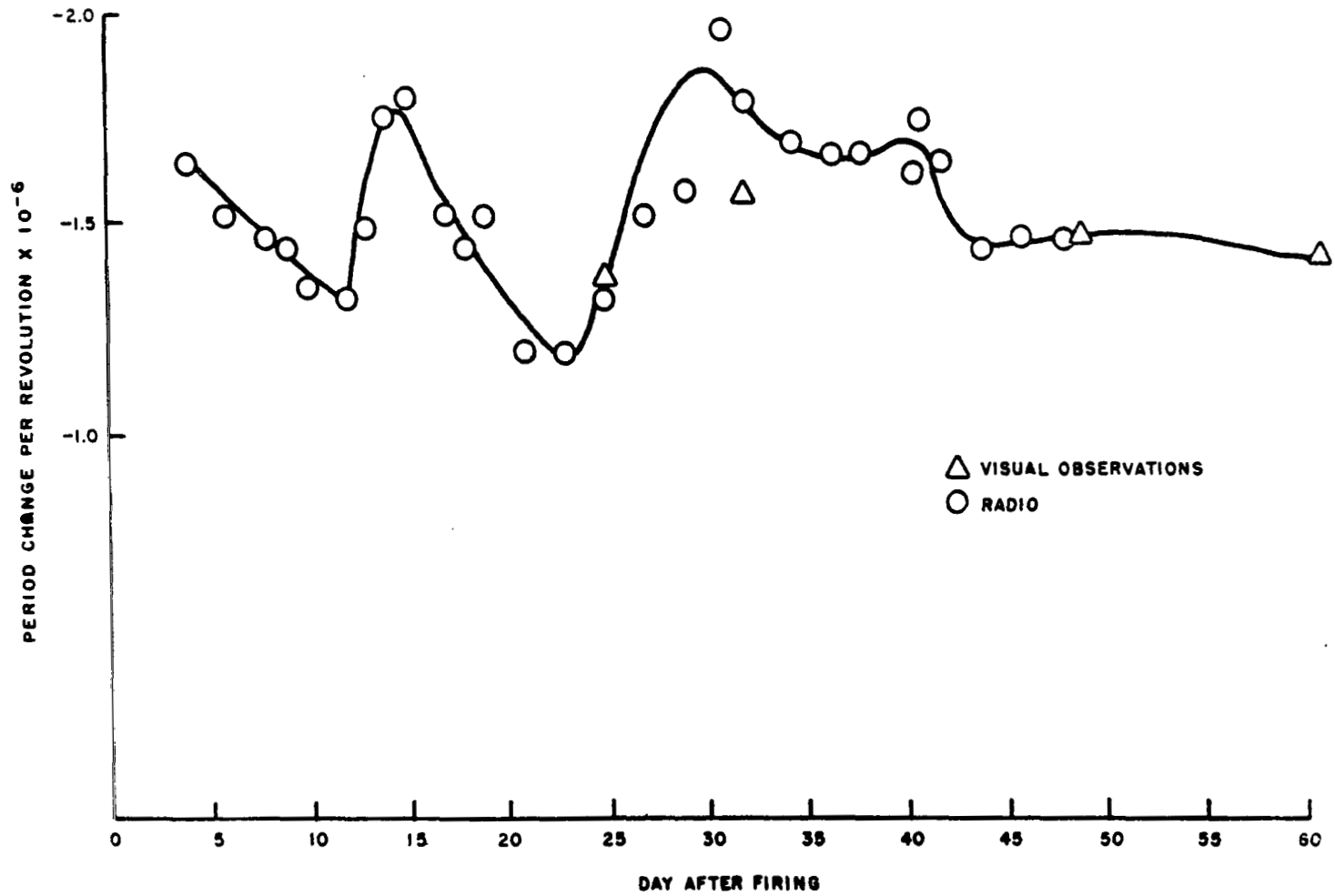


FIGURE 25. CHANGES IN ORBITAL PERIOD OF EXPLORER IV OBSERVED BY LAUTMAN AT SMITHSONIAN ASTROPHYSICAL OBSERVATORY

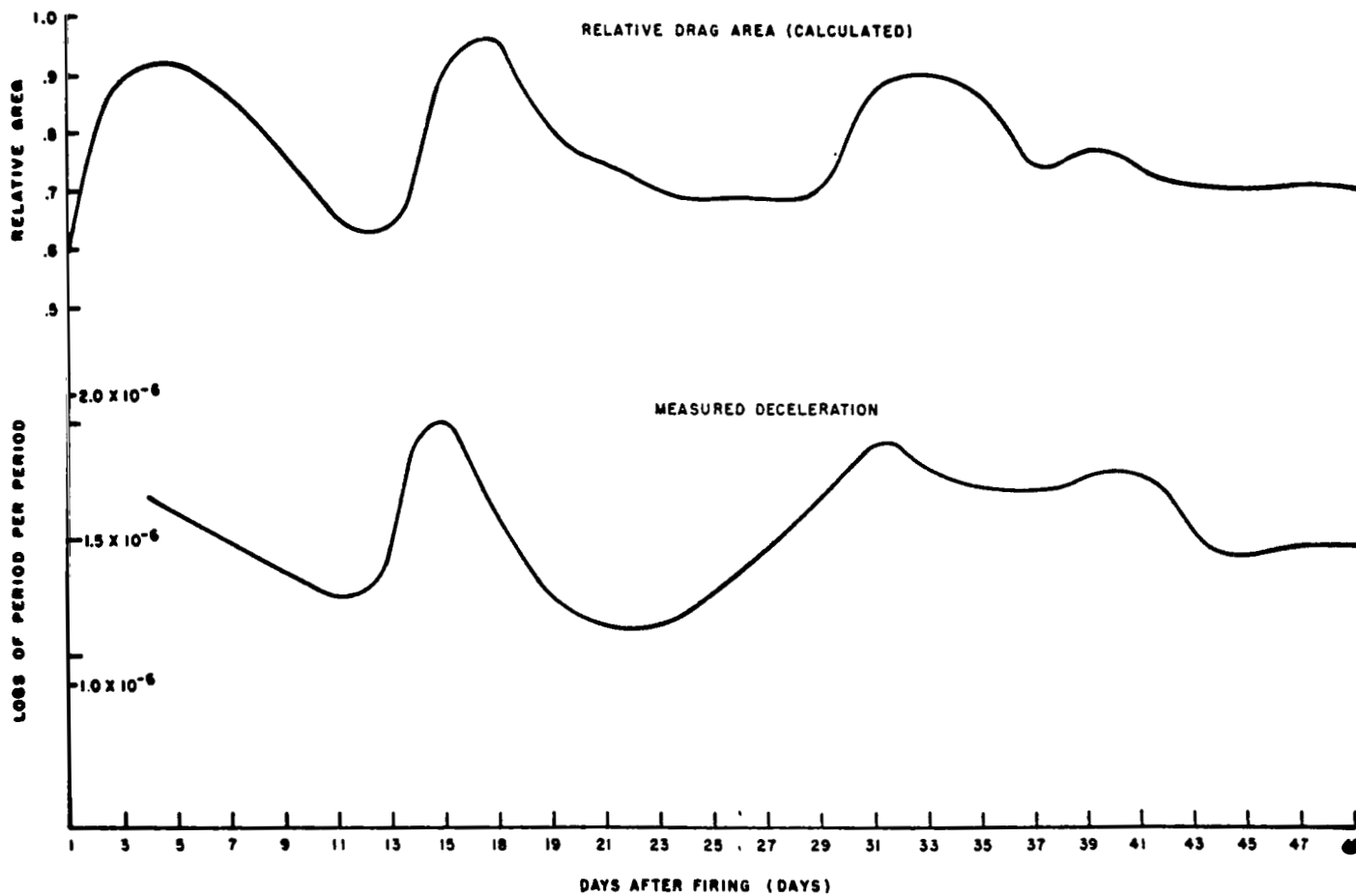


FIGURE 26. COMPARISON OF CALCULATED EFFECTIVE DRAG AREA WITH OBSERVED DRAG DECELERATION

SECTION III. DETERMINING COUNTER ORIENTATION

It was shown by Shelton that the angle the counter axis makes with the magnetic field may be conveniently expressed in an appropriate choice of coordinate systems [Ref. 50]. Let \vec{A} be a unit vector along the satellite symmetry axis and \vec{P} be a unit vector along the counter axis. In a double-primed coordinate system, let \vec{A}'' be along the y'' axis. Since from the geometry of the satellite (Fig. 1) \vec{P} is perpendicular to \vec{A} , \vec{P} will lie in the $x'' - z''$ plane making angle $(\dot{\psi} t + \delta)$ with z'' . The counter axis may then be expressed by

$$\vec{P}'' = \begin{pmatrix} \sin(\dot{\psi} t + \delta) \\ 0 \\ \cos(\dot{\psi} t + \delta) \end{pmatrix} \quad (17)$$

where $\dot{\psi}$ is the roll rate and δ is the roll phase angle or the angle \vec{P} makes y'' at $t = 0$.

Let \vec{B} be a unit vector along the local geomagnetic field at $t = 0$. Consider a primed coordinate system defined such that x' is along the tumble axis \vec{L} and \vec{B} lies in the $x' - y'$ plane. Since \vec{A} is perpendicular to \vec{L} , the symmetry axis is given by

$$\vec{A}' = \begin{pmatrix} 0 \\ \cos(\dot{\phi} t + \gamma) \\ \sin(\dot{\phi} t + \gamma) \end{pmatrix} \quad (18)$$

where ϕ is the tumble rate and γ is the tumble phase angle or the angle \vec{A}' makes with y' at $t = 0$.

The counter axis \vec{P} may be found by

$$\vec{P}' = \begin{pmatrix} 1 & 0 & 0 \\ 0 & \cos(\dot{\phi} t + \gamma) & -\sin(\dot{\phi} t + \gamma) \\ 0 & \sin(\dot{\phi} t + \gamma) & \cos(\dot{\phi} t + \gamma) \end{pmatrix} \begin{pmatrix} \sin(\dot{\psi} t + \delta) \\ 0 \\ \cos(\dot{\psi} t + \delta) \end{pmatrix} \quad (19)$$

Let \vec{B}' have components b_1, b_2, b_3 along $x', y',$ and z' , respectively. The angle λ between the counter axis and the magnetic field is found immediately by

$$\begin{aligned} \cos \lambda = \vec{P}' \cdot \vec{B}' &= b_1 \sin(\dot{\psi} t + \delta) - b_2 \sin(\dot{\phi} t + \gamma) \cos(\dot{\psi} t + \delta) \\ &+ b_3 \cos(\dot{\phi} t + \gamma) \cos(\dot{\psi} t + \delta). \end{aligned} \quad (20)$$

From the equation 20, an idea of the expected periodicity of the counting rate variations may be obtained. The choice of reference time or $t = 0$ is completely arbitrary. At $t = 0$, $b_3 = 0$ from the definition of the primed coordinate system. Then b_1 becomes $\vec{L} \cdot \vec{B}$ and b_2 is $\sqrt{1 - b_1^2}$. If the tumble axis is along \vec{B} , the b_2 term vanishes and λ depends only on ψt . This results in the counting rate being modulated at the roll frequency. However, if \vec{L} is perpendicular to \vec{B} , the b_1 term vanishes and the counting rate will be modulated by the ϕ term when $\cos(\psi t + \delta) \approx 1$. Therefore, periods of tumble modulations will be observed until $\cos(\psi t + \delta)$ becomes small. At these times \vec{P} remains nearly perpendicular to \vec{B} and the counting rate is more or less constant. Such modulations have been observed and pointed out by Van Allen [Ref. 51].

From this expression the angle λ may be found at various times during a particular pass if ϕ , ψ , γ , δ , b_1 , b_2 , and b_3 are known. The b_1 , b_2 , and b_3 may be found from the \vec{L} and \vec{B} by

$$\begin{pmatrix} b_1 \\ b_2 \\ b_3 \end{pmatrix} = \begin{pmatrix} L_x & L_y & L_z \\ \frac{\bar{B}_x - KL_x}{\sqrt{1-K^2}} & \frac{\bar{B}_y - KL_y}{\sqrt{1-K^2}} & \frac{\bar{B}_z - KL_z}{\sqrt{1-K^2}} \\ \frac{L_y \bar{B}_z - L_z \bar{B}_y}{\sqrt{1-K^2}} & \frac{L_z \bar{B}_x - L_x \bar{B}_z}{\sqrt{1-K^2}} & \frac{L_x \bar{B}_y - L_y \bar{B}_x}{\sqrt{1-K^2}} \end{pmatrix} \begin{pmatrix} B_x \\ B_y \\ B_z \end{pmatrix} \quad (21)$$

where B_x , B_y , B_z are the normalized components of the field in a vernal equinox coordinate system and $K = \vec{L} \cdot \vec{B}$. The Smithsonian ephemeris lists the satellite position and the local geomagnetic field components in one-minute intervals throughout the transmitter lifetime. These magnetic field components are expressed in gauss and resolved in terms of a local vertical system in which B_D is antiparallel to the local vertical, B_E is perpendicular to the local vertical and extends to the east, and B_N is mutually perpendicular to B_D and B_E and is directed to the north. These components may be transformed into the vernal equinox system by

$$\begin{pmatrix} B_x \\ B_y \\ B_z \end{pmatrix} = \begin{pmatrix} \frac{-R_x R_z}{\sqrt{R_x^2 + R_y^2}} & \frac{R_y}{\sqrt{R_x^2 + R_y^2}} & -R_x \\ -\frac{R_y R_z}{\sqrt{R_x^2 + R_y^2}} & \frac{R_x}{\sqrt{R_x^2 + R_y^2}} & -R_y \\ \sqrt{R_x^2 + R_y^2} & 0 & -R_z \end{pmatrix} \begin{pmatrix} B_N \\ B_E \\ B_D \end{pmatrix} \quad (22)$$

where R_x , R_y , R_z are the direction cosines of the radius vector from the center of the earth to the satellite in the vernal equinox coordinate system. The quantities B_N , B_E , and B_D are the normalized components of the magnetic field as given in the Smithsonian ephemeris.

The tumble rate and phase may be found by making use of the nose and tail radio frequency radiation pattern nulls observed in the signal strength recordings. As discussed in Chapter II, the nose nulls are identifiable by the small lobes that appear on either side of the null. The observation of the null in the radio frequency radiation pattern along the nose or tail of the satellite occurs when the axis of symmetry makes the closest approach to the sight vector \vec{U} . The axis of symmetry at the observance of a null is given by

$$\vec{A} = \pm \frac{(\vec{L} \times \vec{U}) \times \vec{L}}{|\vec{L} \times \vec{U}|} \quad (23)$$

where the minus sign is taken for a nose null and a plus sign for a tail null.

The angle through which the satellite has tumbled between the time of the first null and the time of the i^{th} null is

$$\dot{\phi} t_i - \phi_0 = 2 n \pi \pm \arccos (\vec{A}_1 \cdot \vec{A}_i) \quad (24)$$

where t_i is the time of the i^{th} null after the reference time and where n is the number of revolutions the satellite has made between the first and the i^{th} null. The angle ϕ_0 is the angular displacement of \vec{A}_1 at $t = 0$. The sign of the arccosine term depends on the sense of the tumble and the angular component of the \vec{U} .

The times at which nose or tail nulls were observed were then found during a particular pass, the \vec{A}_i at each null was computed, and the angle through which the satellite had tumbled since the first null was found. If the tumble rate is assumed constant during a pass, the angular displacement must be a linear function of time. Imposing this requirement, the angular displacement was fit to a first degree polynomial by the method of least squares. The constant term is therefore the initial angular displacement ϕ_0 and the first power coefficient is the angular rate $\dot{\phi}$.

The accuracy of this determination should be emphasized. The primary source of error in this measurement is the time of the observance of the null. Since a time signal from WWV was recorded on the strip chart containing the telemetry, these times are probably accurate to .1 second. The arccosine term in equation 24 is generally less than .001 revolution per tumble cycle. Therefore, the uncertainties in \vec{L} are not significant. The error in $\dot{\phi}$ resulting from an error in t is

$$\Delta \dot{\phi} = \dot{\phi} \frac{\Delta t}{t} \quad (25)$$

so that the error is reduced by measuring over a long interval t . In general, the time available for observing nose and tail nulls is on the order of 5 minutes. An uncertainty of .2 seconds in determining the interval t between the first and last null corresponds to 1 part in 1500. Since the tumble rate $\dot{\phi}$ is approximately a radian per second, the maximum error in $\dot{\phi}$ is a milliradian per second. Since least square fitting was employed, the error in $\dot{\phi}$ is probably on the order of $\pm .0001$ rad/sec. Figure 27 shows the values of $\dot{\phi}$ obtained from August 27 through September 1. It may be seen that the tumble rate is slowly decaying, having lost approximately .008 rad/sec in 5 days. This loss can be attributed to damping by both the atmosphere and the geomagnetic field. However, the decay rate corresponds to a loss of 10^{-5} rad/sec during a pass and does not invalidate the assumption that $\dot{\phi}$ is constant during a pass.

This same accuracy is also retained in the phase angle ϕ_0 . From this phase angle, the components of the symmetry axis, \vec{A} , at $t = 0$ may be found by

$$\vec{A} = \begin{pmatrix} A_{1x} \cos \phi_0 - (L_y A_{1z} - L_z A_{1y}) \sin \phi_0 \\ A_{1y} \cos \phi_0 - (L_z A_{1x} - L_x A_{1z}) \sin \phi_0 \\ A_{1z} \cos \phi_0 - (L_x A_{1y} - L_y A_{1x}) \sin \phi_0 \end{pmatrix} \quad (26)$$

where A_{1x} , A_{1y} , A_{1z} are the components of \vec{A} at the first null. Since γ was defined to be the angle the symmetry axis makes with the y' axis at $t = 0$,

$$\cos \gamma = \frac{(\vec{L} \times \vec{B}) \cdot \vec{L}}{|\vec{L} \times \vec{B}|} \cdot \vec{A} \quad (27)$$

The quadrant of γ may be determined by inspection.

The determination of $\dot{\phi}$ and γ thus far is completely independent of any assumption on the distribution of trapped particle flux. There is, however, still the ambiguity in the sense of tumble. Examination of the counting rate data reveals two important observations. During times that \vec{L} is nearly perpendicular to \vec{B} , sharp peaks in counting rate are observed at 3.5-second intervals. Also, the peaks in counting rate are immediately preceded by a nose or tail null. If a particle is trapped on a line of force, the acute angle α that its velocity vector makes with a line of force as it approaches the satellite should be independent of the direction in which the guiding center moves along the line of force. Therefore, the distribution of trapped particle flux should be symmetrical about a plane perpendicular to the magnetic field. The angle λ_p that the counter axis makes with the magnetic field when a sharp counting peak is observed may be found by neglecting b_1 and b_3 in equation 20, or

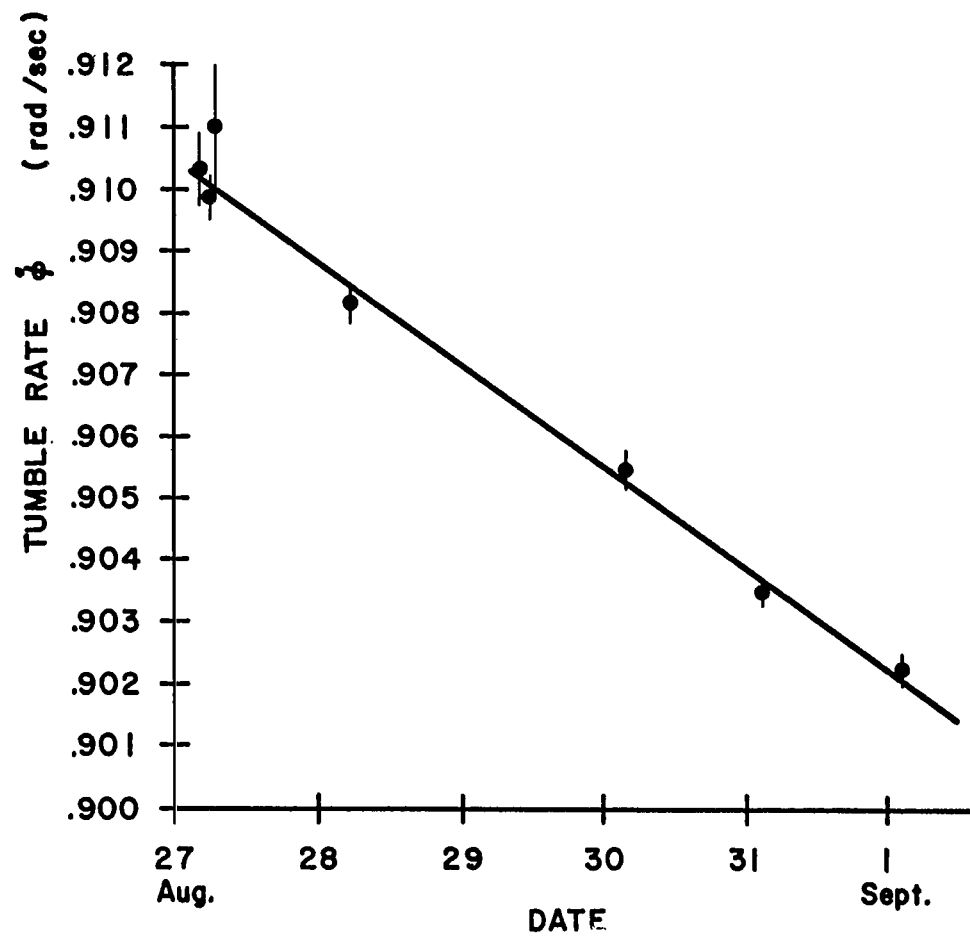


FIGURE 27. OBSERVED TUMBLE RATES FROM AUGUST 27 THROUGH SEPTEMBER 1

$$-\cos \lambda_p = \sin (\dot{\phi} t + \gamma) \cos (\dot{\psi} t + \delta) \quad (28)$$

In the interval of interest, $\phi \gg \dot{\psi}$, and $\cos (\dot{\psi} t + \delta)$ may be considered constant during a cycle of ϕ . From the argument that the flux distribution is symmetrical about a plane perpendicular to \vec{B} , a counting rate peak must be observed at $+\cos \lambda_p$ as well as at $-\cos \lambda_p$. In general, four such peaks should be observed during a tumble cycle unless λ_p is 0 or $\pi/2$. Since particles whose velocity vectors lie along lines of force are not trapped, and since only 2 counting rate peaks are observed during a tumble cycle, it is concluded that the peak intensity is observed when $\lambda = \pi/2$ ¹. This results in counting rate peaks occurring when the symmetry axis is along the magnetic field line for the case where \vec{B} is nearly perpendicular to \vec{L} . This result, together with the observation that a nose or tail fade occurs just prior to a counting rate peak, allows the direction of the tumble to be determined. The geometry of the passes during the period of interest (August 27 through September 1) was such that the satellite rose above the radio horizon just after crossing the equator. The tumble axis was indeed almost perpendicular to the line of sight and to the magnetic field, and was almost along the line of equinoxes. Figure 28 shows the relationship of the line of sight and \vec{B} . Since a nose or tail null was observed as the symmetry axis passed the line of sight just prior to the observance of a peak counting rate as the symmetry axis passes \vec{U} , it is concluded that the angular momentum vector must be in the direction of the vernal equinox.

The task of determining the roll rate and phase remains. Since it is not possible to infer roll from the signal strength, it becomes necessary to make use of the counting rate data. In the first case where $b_1 \ll b_2$,

$$|\cos \lambda| = [b_2 \sin (\dot{\phi} t + \gamma) - b_3 \cos (\dot{\phi} t + \gamma)] \cos (\dot{\psi} t + \delta). \quad (29)$$

During the period of continuous high counting rate extending over several tumble cycles, it is presumed that λ remains nearly $\pi/2$ independent of ϕ . This may happen only if $\cos (\dot{\psi} t + \delta)$ becomes small or $\dot{\psi} t + \delta \approx (2n-1) \pi/2$. The times of such occurrences during a pass are noted, and the angular displacement of $\dot{\psi} t + \delta$ is taken to be $(2n-1) \pi/2$ at the times of the midpoints of such occurrences. Again employing the assumption of uniform rotation during the pass, the angular displacements are fit to a first degree polynomial by the method of least squares. In this manner the rate $\dot{\psi}$ and the phase may be readily found.

1. This does not necessarily imply that the intensity of particle flux is maximum at 90° to the field. Since the counter has a finite resolution, a peak counting rate at $\lambda = 90^\circ$ may be observed if the peak in particle flux is sufficiently close to 90° to be within the resolution of the detector.

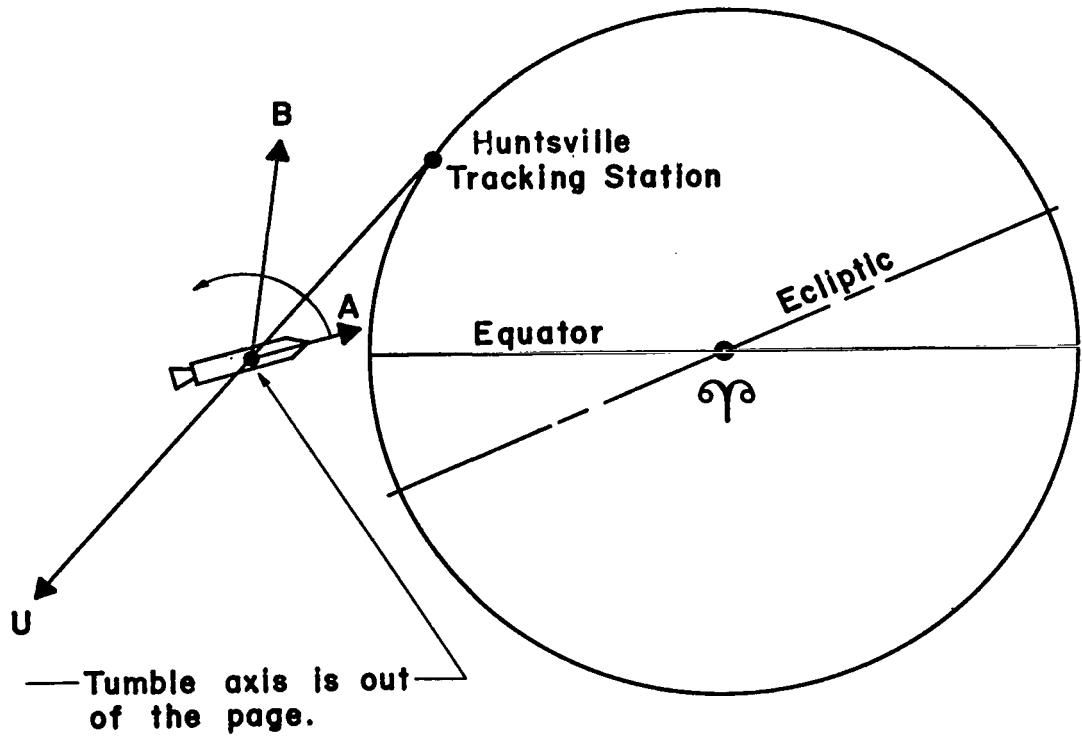


FIGURE 28. GEOMETRY OF A TYPICAL PASS AT ACQUISITION DURING THE PERIOD FROM AUGUST 27 TO SEPTEMBER 1

If b_1 is not small compared to b_2 , $\dot{\psi}$ and δ may be determined by observing times of peak counting rates and equating $\cos \lambda$ to 0 in equation 20 at these times. The resulting equation may be solved for $\dot{\psi} t + \delta$ giving

$$\left| \tan (\dot{\psi} t + \delta) \right| = \frac{b_2 \sin (\dot{\phi} t + \gamma) - b_3 \cos (\dot{\phi} t + \gamma)}{b_1} . \quad (30)$$

From several counting rate peaks, various values of $\dot{\psi} t + \delta$ may be found at various times. Again, the least square fit of this data to a first degree polynomial may be used to obtain $\dot{\psi}$ and δ .

Again there is an ambiguity in the sign of $\dot{\psi}$. As long as the b_1 term remains small, $\cos \lambda$ depends only on $\cos (\dot{\psi} t + \delta)$ and the sign of $(\dot{\psi} t + \delta)$ is immaterial. This is generally the case in the passes analyzed. The calculations were performed assuming both positive and negative roll directions at times when b_1 was the largest. It appeared that the positive value for roll yielded a better fit to the radiation data, but b_1 never became large enough to determine this definitely.

SECTION IV. RESULTS AND CONCLUSIONS

A. ANALYSIS OF OBSERVED RADIATION

Having developed a procedure in the previous chapter whereby the counter orientation may be determined as a function of time, particular passes during the period from August 27 to September 1 were selected for analysis. This period was chosen because it included the first two Argus events and the records were of exceptional quality. Unfortunately, the Channel 2 subcarrier oscillator ceased operation on September 2, shortly before the third Argus event; hence, no directional counter data is available after this date.

In selecting the passes for this analysis, several requirements had to be considered. First and most important, the radiation counting rate had to be high enough so that the accumulation time of the counter was short compared to a tumble cycle. In general, two passes each day met this requirement. Second, the pass must have readable time scales. Third, the pass must have readable radio frequency signal strength recordings in order to determine the tumble rate and phase. Eight passes were selected during the time from August 27 to September 1 that met these requirements. They are passes 414, 415, 416, 428, 453, 454, 466, and 479.¹

The Channel 2 counting rate was read using a Universal Telereader in conjunction with an IBM card punch. The distance on the telemetry record from a reference point to each switch of the subcarrier oscillator was read and punched into an IBM card. In a similar manner the distance between two known times was recorded on an IBM card. These cards were used in a computer program that converted the location of a switch of the subcarrier oscillator frequency into time after the reference point, determined the time interval between successive switches, and divided this time into the counter scale factor. The resulting count rate is taken to be effective at the midpoint of the interval between the successive switches. This time and the corresponding counting rate were then recorded on magnetic tape. To prevent cumulative time errors, a new reference time is taken every 15 seconds during the pass from the WWV time scales. Further error analyses follow in part B of this section.

The times of occurrences of the signal strength fades because of the nose and tail nulls were determined and the ϕ , ψ , γ , and δ were calculated as outlined in Section III. These inputs along with the reference time and the components of \vec{L} were

1. The pass numbering convention used here takes the first ascending node as the beginning of Pass 1. Passes are then numbered successively at each subsequent ascending node.

then fed into a computer program which contained the orbital elements and the coefficients for the magnetic field expansion. The magnetic tape containing times and the corresponding counting rates was then read by the computer and the angle λ for each time was computed and listed with the corresponding counting rate.

Figures 29 through 31 show the observed counting rate as a function of time together with the computer λ as a function of time. Note the counting rate peaks that are due to tumble modulations appear to coincide quite well with the $\lambda = 90$ degrees points. It should be remembered that the tumble rate and its phase determination is completely independent of the radiation counting rates except for the geometric argument for the direction of rotation.

Figures 32 through 37 are plots of the observed counting rates as functions of λ . Some scatter of points is observed and data smoothing techniques must be employed to find the best fit to this data. The degree of uncertainty associated with these points will be discussed in the following section. The smoothed data may then be corrected for counter dead time according to equation 12 to obtain the true count rate as a function of λ .

Examination of the counting rate versus λ plots reveals a plateau of almost uniform low counting rates from $\lambda = 0$ degree to about 50 degrees. This is probably due to trapped particles that are energetic enough to penetrate the walls and intervening material of the payload and be counted regardless of the counter axis orientation.

The plots of counting rate versus λ that are included herein are taken from only one of the passes analyzed. They are intended as a representative sample of the results obtained from this study. The plots for the other passes will be published separately.

B. ERROR ANALYSIS

Having obtained values of counting rate for various values of λ , the accuracy of this determination must be investigated. Three sources of error are present in this analysis: error in reading the counting rate, error in establishing the time corresponding to a particular counting rate, and error in determining λ as a function of time.

The error in obtaining the counting rate becomes significant when the counting rate becomes high. Since the data are represented by a series of square waves whose periods are the time required to collect 2048 counts, a counting rate on the order of 6000 counts sec^{-1} results in this square wave having a half period of approximately .16 second. The original data was recorded on strip charts with a paper speed of approximately .7 cm/sec. Hence, the subcarrier oscillator switches frequency every .16 second which corresponds to approximately 1 mm on the recorded strip chart. The location of these switches are probably not determined to better than $\pm .1$ mm by the

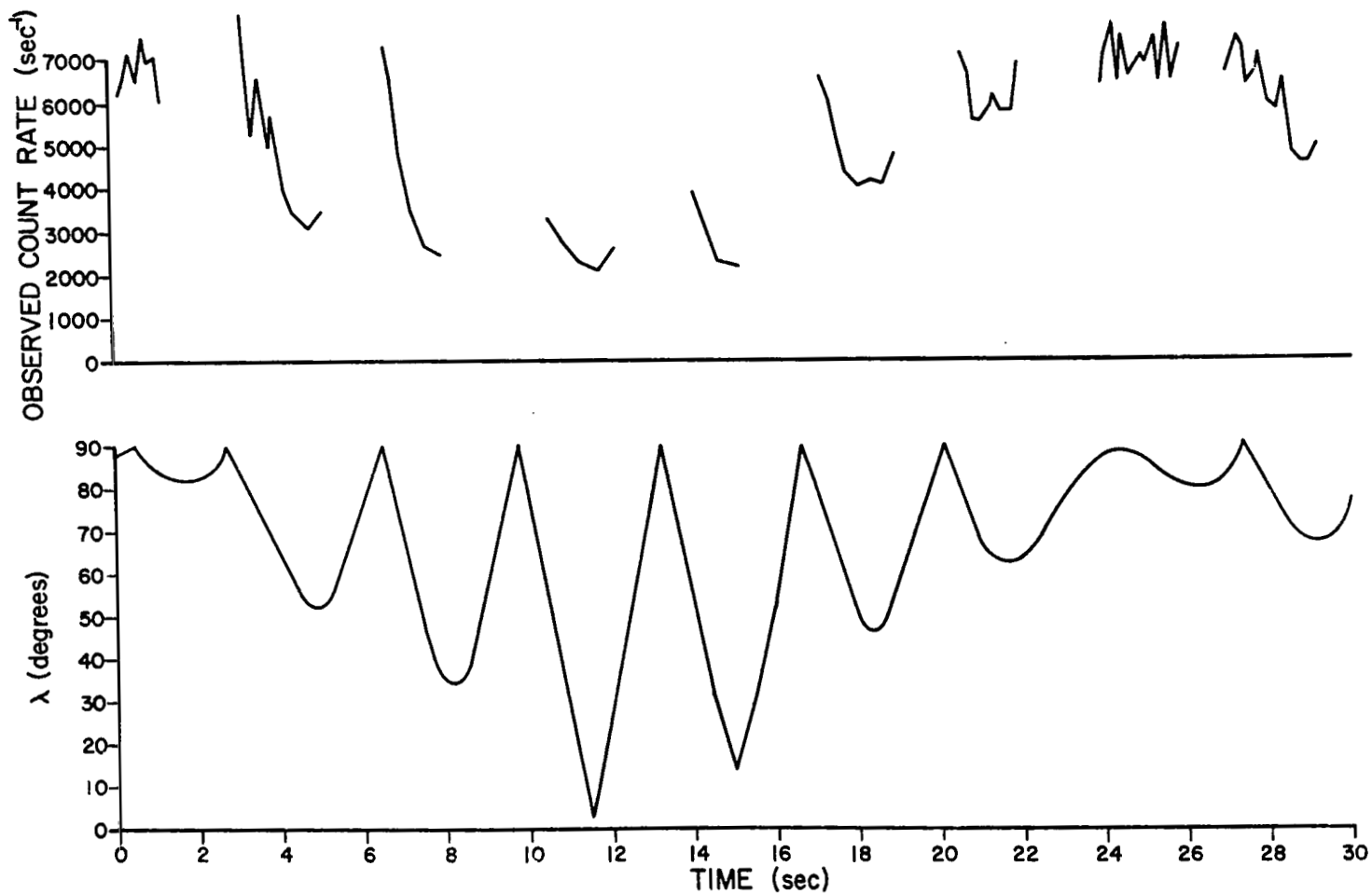


FIGURE 29. COMPARISON OF OBSERVED COUNTING RATES WITH THE CALCULATED λ DURING THE INTERVAL 0500:00 to 0500:30 UT ON AUGUST 30.

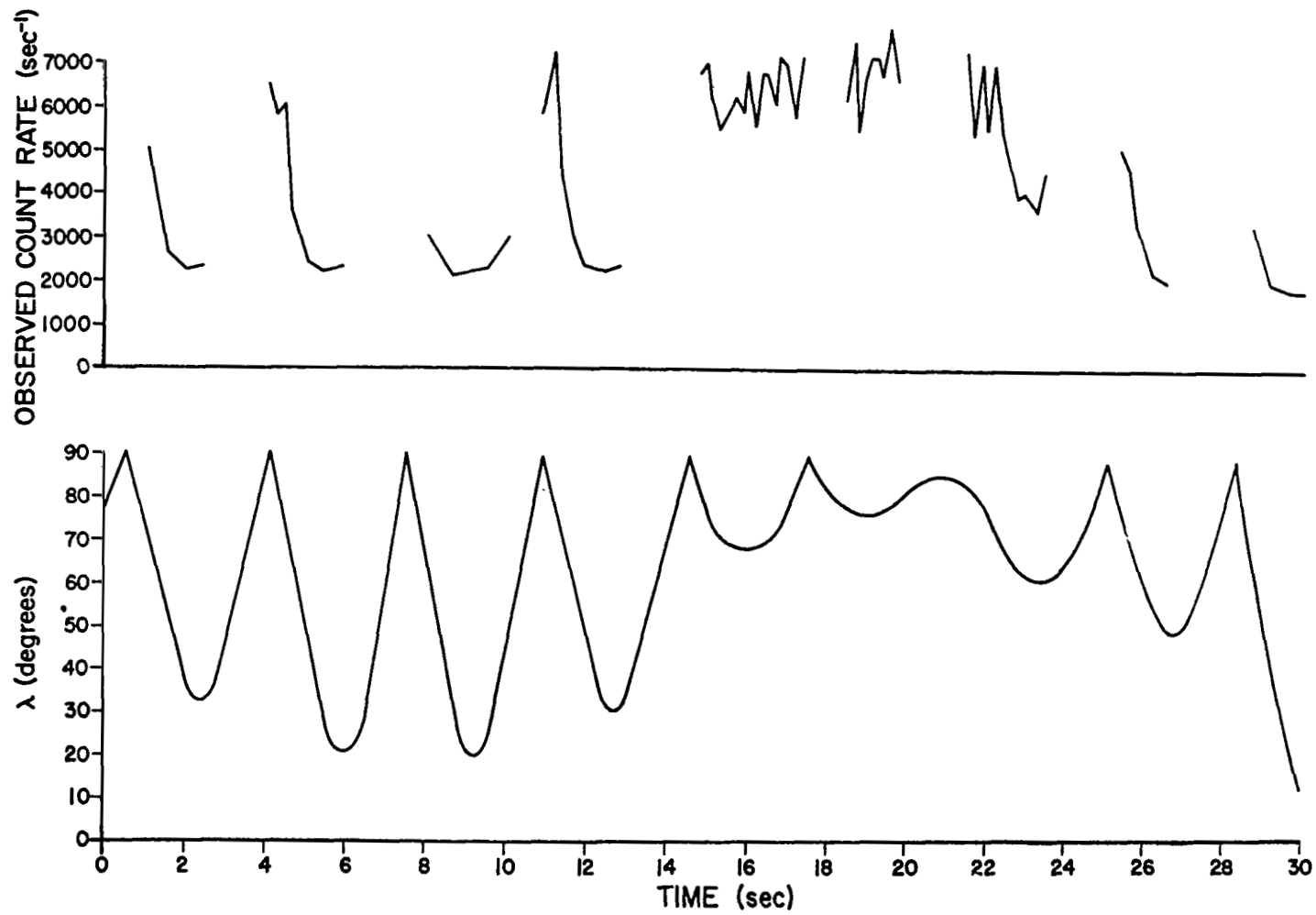


FIGURE 30. COMPARISON OF OBSERVED COUNTING RATES WITH THE CALCULATED λ DURING THE INTERVAL 0500:30 TO 0501:00 UT ON AUGUST 30.

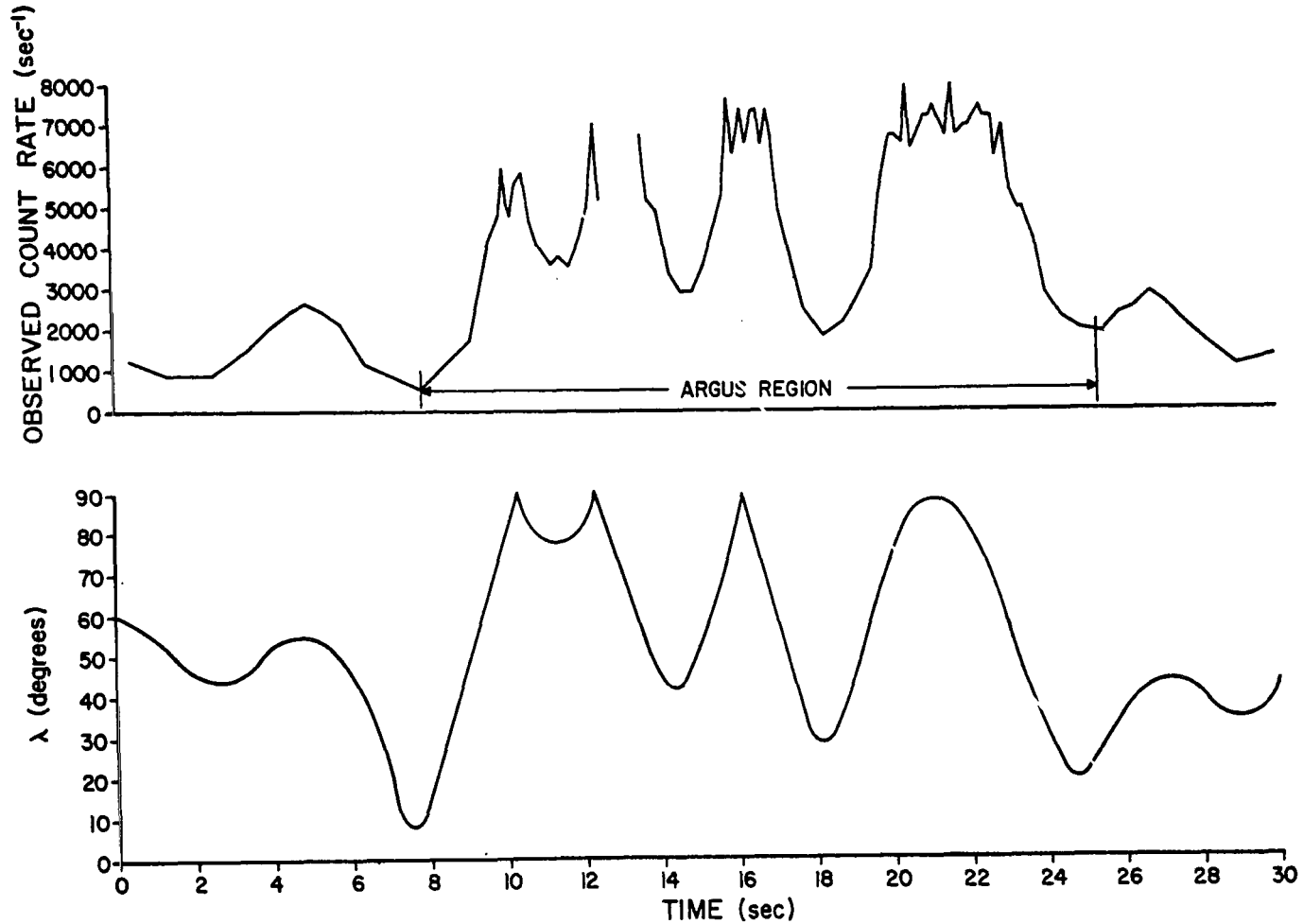


FIGURE 31. COMPARISON OF OBSERVED COUNTING RATES WITH THE CALCULATED λ DURING THE INTERVAL 0510:00 TO 0510:30 UT ON AUGUST 30. THE PERIOD OF HIGH COUNTING RATE IS DUE TO A PASSAGE OF THE SATELLITE THROUGH AN ARGUS SHELL

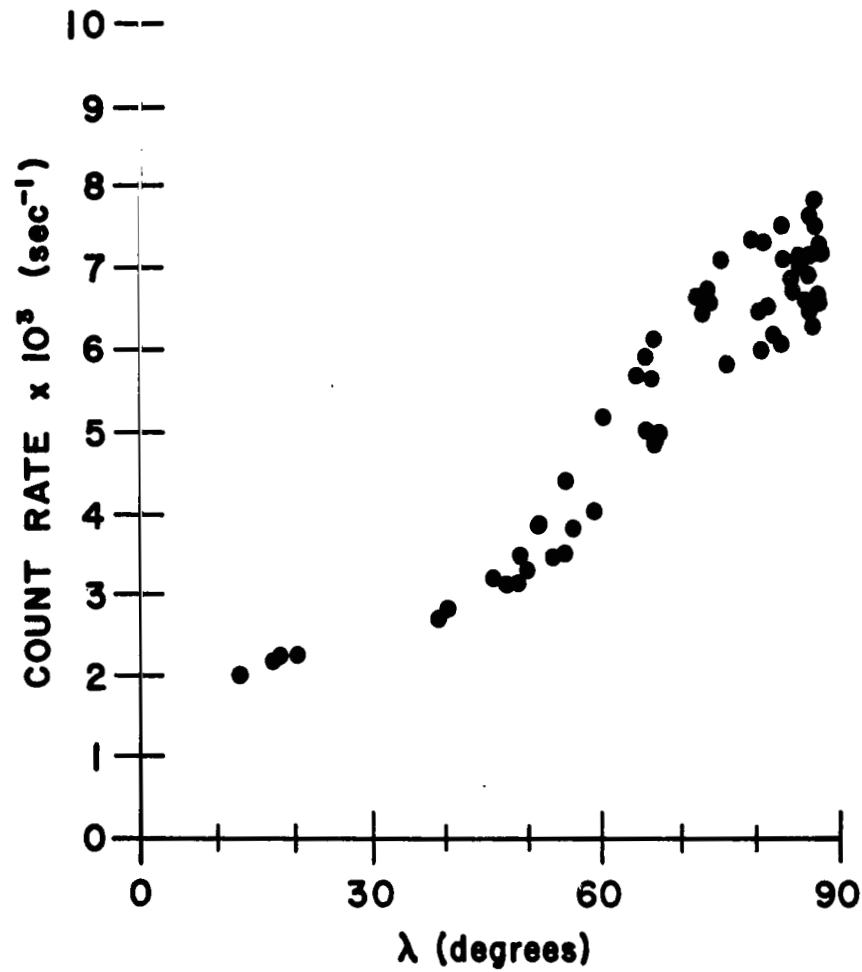


FIGURE 32. COUNTING RATE VERSUS λ FOR 0500:00 TO 0500:30 UT, AUGUST 30, 1958

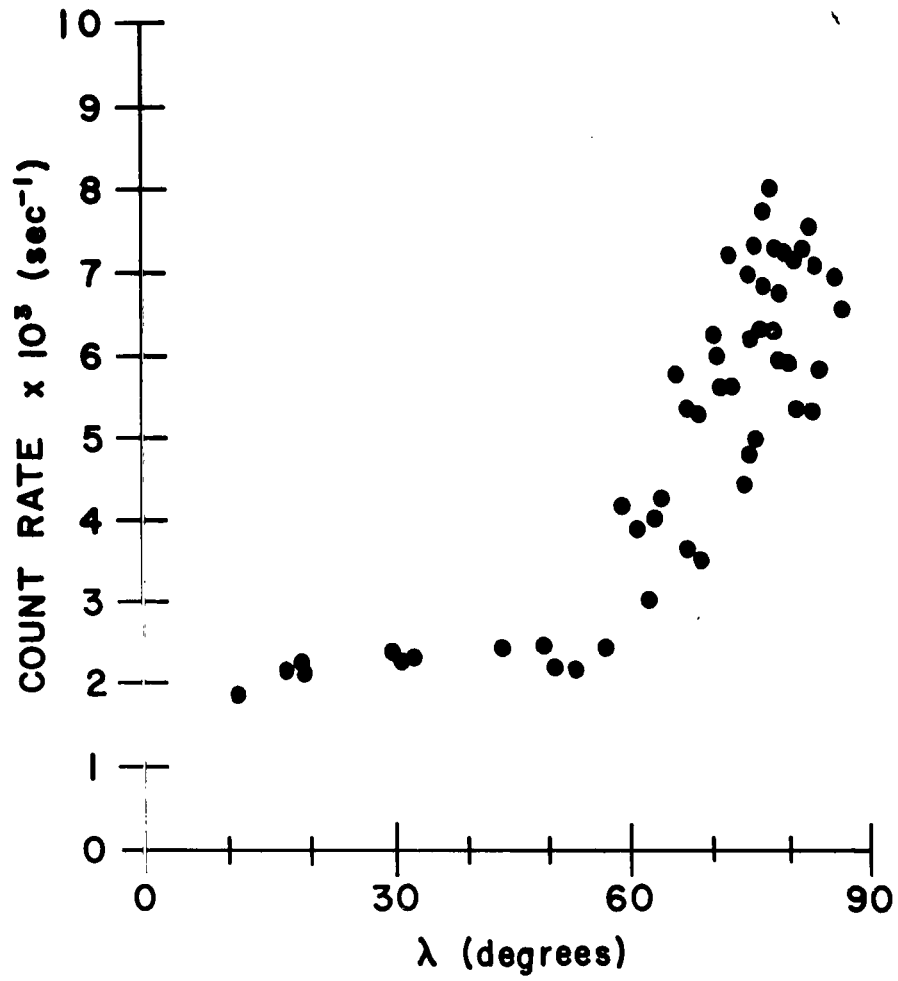


FIGURE 33. COUNTING RATE VERSUS λ FOR 0500:30 TO 0501.00 UT, AUGUST 30, 1958

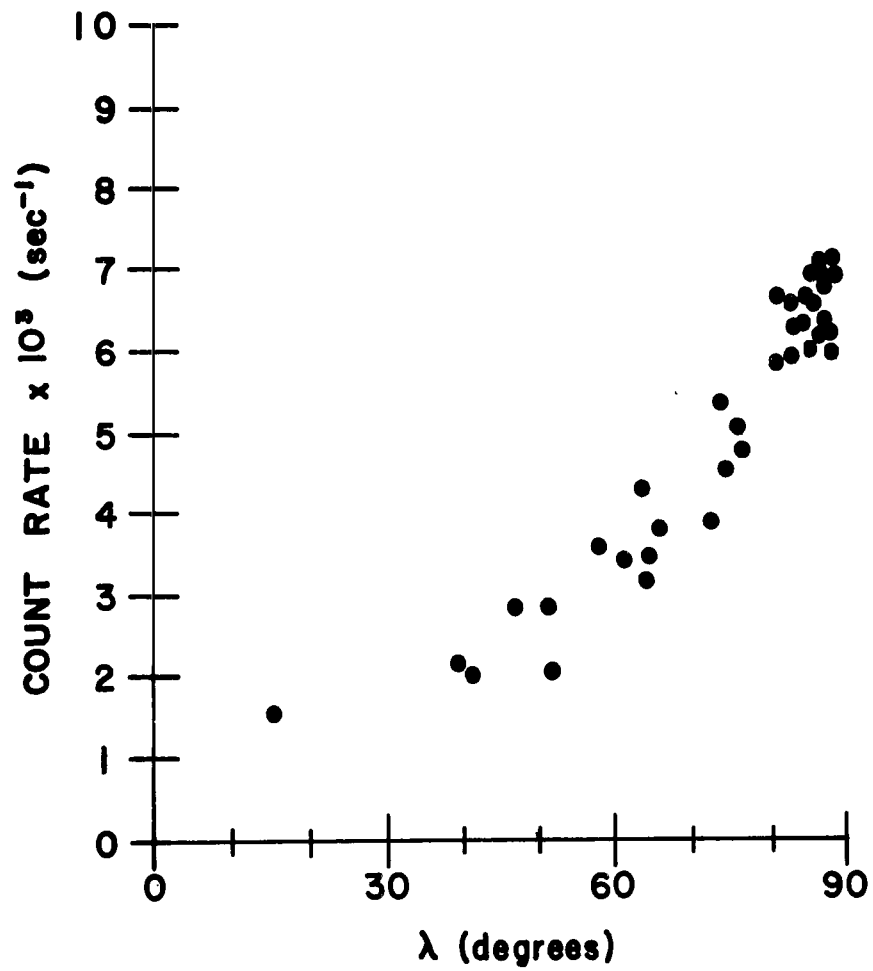


FIGURE 34. COUNTING RATE VERSUS λ FOR 0501:00 TO 0501:30 UT, AUGUST 30, 1958

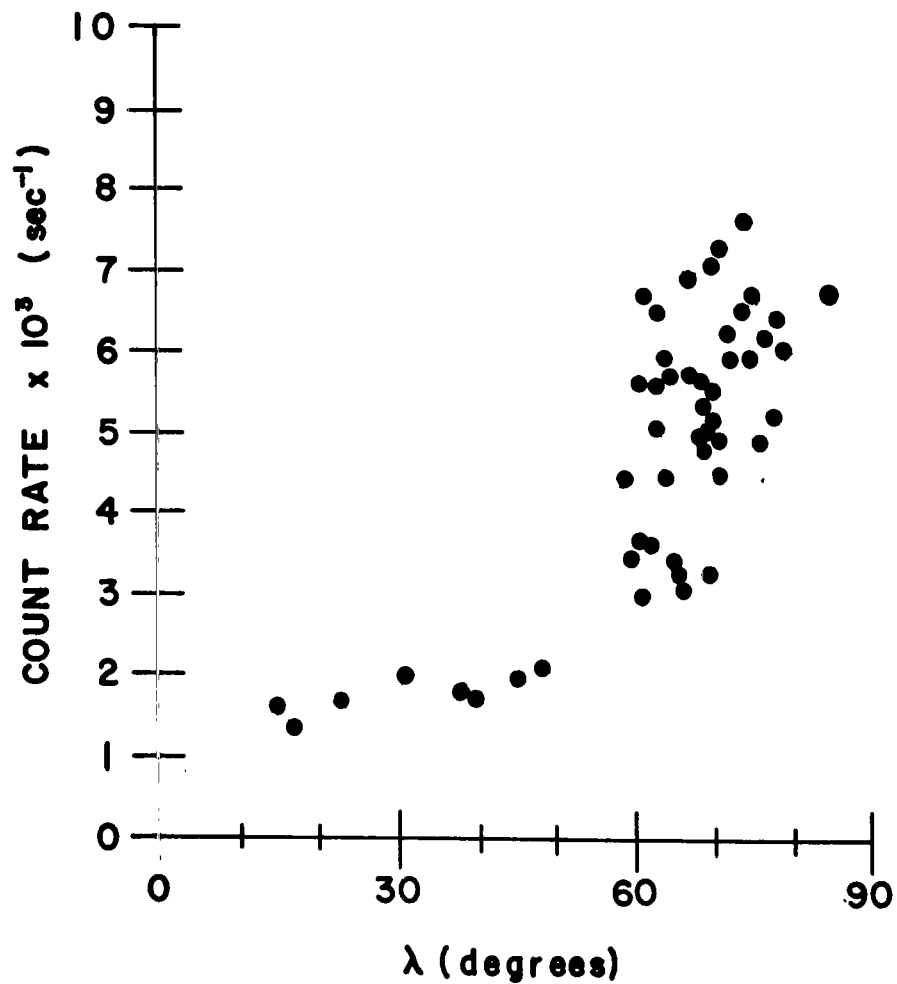


FIGURE 35. COUNTING RATE VERSUS λ FOR 0501:30 TO 0502:00 UT, AUGUST 30, 1958

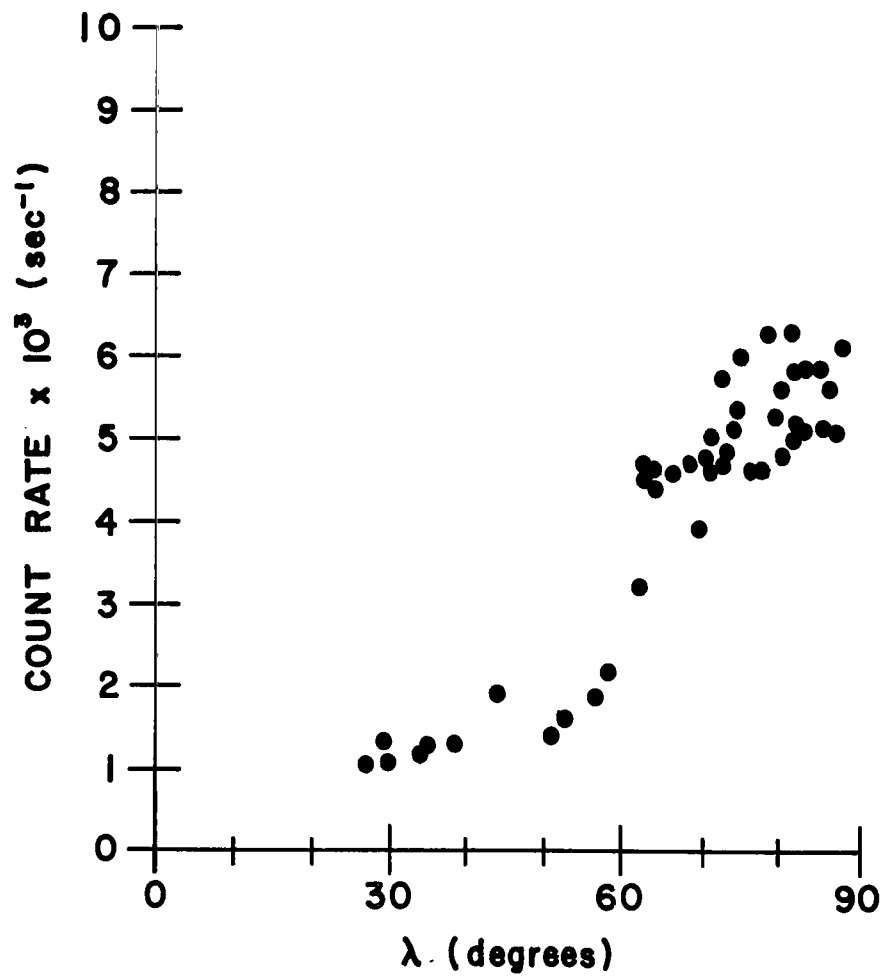


FIGURE 36. COUNTING RATE VERSUS λ FOR 0502:30 TO 0503:00 UT, AUGUST 30, 1958

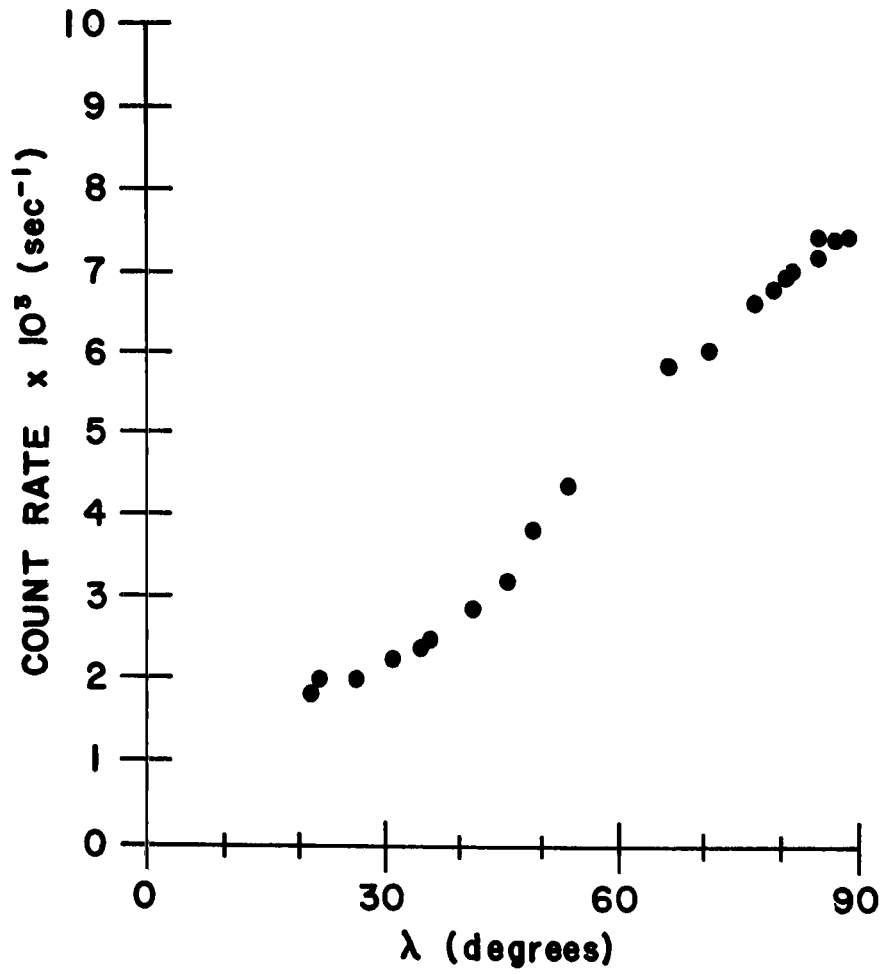


FIGURE 37. COUNTING RATE VERSUS λ FOR 0510:07 TO 0510:25 UT, AUGUST 30, 1958

method used; hence, for high counting rates, the observed value may be in error by ± 10 per cent. Since this error is random and not cumulative, smoothing techniques may be used. This error could be reduced by playing back the original magnetic tapes and recording the data at a higher paper speed. A speed of 2 cm/sec should reduce this error to about ± 3 per cent.

The second source of error lies in establishing the times at which the counting rates are determined. Some variation in the paper speed at which the strip charts were recorded was noted. To minimize this error, new reference times were taken every 15 seconds along the chart. It is believed that the variation in paper speed during a 15-second interval is not significant. However, these reference times cannot be located relative to Universal Time more accurately than to the nearest .1 second, and at times when WWV is not clearly readable this precision cannot be guaranteed. During times when tumble modulations are present in the counting rate data, the counter axis may be moving relative to \vec{B} at the rate of 60 deg/sec. A .1-second error in time results in an error in λ of about six degrees.

The assumption that the observed counting rate corresponds to the midpoint between the two successive switches in the subcarrier oscillator frequency may also lead to a time error, particularly if the counting rate is changing rapidly. This error will be much less than the time interval between the two switches; therefore, for high counting rates this error will be less than .1 second in time. For low counting rates, this error becomes greater, but low counting rates generally occur at small values of λ . From the plots of counting rate versus λ it was seen that counting rate is almost independent of λ for $0^\circ < \lambda < 50^\circ$; hence, this error may be disregarded.

The final source of error lies in computing λ as a function of time. The accuracy of this calculation obviously depends on the uncertainties in parameters ϕ , ψ , γ , δ , b_1 , b_2 , and b_3 . The accuracy of ϕ has already been stressed. This is the most important parameter since cumulative errors may arise from this term. If $\dot{\phi}$ is accurate to $\pm .0001$ rad/sec, the resultant error in λ will be less than four degrees after ten minutes.

Since $\dot{\psi} \ll \dot{\phi}$, the accuracy requirements on ψ are not nearly as severe. In the cases where b_1 is small, all that is required of the $\dot{\psi}$ term is to produce the long periods of nearly constant counting rates observed in the data. Since $\dot{\psi}$ and δ were obtained by fitting the observed counting rate data over the interval of interest with the condition that $\dot{\psi}$ is constant, errors in these values will be neglected. It can be said that the requirement that $\dot{\psi}$ be constant was consistent with the observed periods of counting rates where tumble modulations were not observed.

The phase angle γ involves the tumble axis \vec{L} which has a fairly large uncertainty. However, the geometry of the \vec{L} , \vec{U} , and \vec{B} during the passes of interest is such that γ is quite insensitive to errors in the orientation of \vec{L} . The change in γ resulting from a ten-degree variation in the right ascension and declination of \vec{L} is on the

order of one degree, and will be neglected. An error in γ results essentially in a time displacement of λ .

The uncertainty in \vec{L} will also result in uncertainties in the b_1 , b_2 , and b_3 coefficients. Since $t = 0$ may be taken arbitrarily, $b_3 = 0$, $b_1 = \cos \beta$, and $b_2 = \sin \beta$ where β is the angle \vec{B} makes with \vec{L} . In the passes examined, by chance, β was nearly $\pi/2$. Hence, when $\sin(\psi t + \delta)$ is nearly unity, $\lambda \approx \beta$, and the uncertainty in λ is the same as in β or about ten degrees. On the other hand, when $\cos(\psi t + \delta)$ is nearly unity, λ is little affected by β when $\sin(\phi t + \gamma)$ is small. When $\sin(\phi t + \gamma)$ is nearly unity, $\lambda \approx \pi/2 - \beta$. Hence, during the tumble modulations, λ is well determined near $\pi/2$. The minimum value that λ reaches is subject to the same uncertainties involved in the \vec{L} . Again, the fact that the radiation counting rate is insensitive to λ for angles less than 50 degrees minimizes the effect of this error.

C. CONCLUSIONS

It has been demonstrated that the determination of the time dependence of the plane of tumble of Explorer IV has been successful in explaining the observed temperature variations, the observed drag accelerations, and the radiation counting rate modulations observed by the directional scintillation detector. Furthermore, counting rate as a function of angle that the scintillation counter axis makes with the magnetic field has been determined at various points in the geomagnetic field. It has been shown that the counting rate is a maximum when the detector is perpendicular to the magnetic field and that the counting rate falls to a uniform value at angles less than about 40 degrees through 50 degrees to the field. From the angular dependence of the counting rate, the angular distribution of the trapped particle flux may be obtained which will permit calculation of the intensity at each subsequent mirror point along the line of force.

Two interesting effects were also observed during the course of this study. The first, which was originally observed by Fields, was that the roll required to explain the periodicity of the occurrences of intervals where the counting rate is not modulated by the tumbling motion appeared to vary from day to day. The results of these observations, shown in Figure 4, indicate that the roll actually increases by almost an order of magnitude on August 28. The roll rate increase observed on this date represents an angular momentum increase of $10^5 \text{ gm cm}^2 \text{ sec}^{-1}$. It is not possible to determine whether total angular momentum is conserved and whether the increase in longitudinal angular momentum results from a decrease in transverse or tumble angular momentum, or if external torques are acting about the symmetry axis. A gain of $10^5 \text{ gm cm}^2 \text{ sec}^{-1}$ about the longitudinal axis would result in a decrease in $\dot{\phi}$ of approximately $.2 \times 10^{-4} \text{ rad/sec}$ if total angular momentum is to be conserved. This value is less than the uncertainty in $\dot{\phi}$. If external torques are responsible for the roll rate increase, a continuous torque on the order of one dyne-cm would be required.

The second interesting and somewhat surprising result is that the angular momentum vector does indeed appear to change orientation by as much as 10 degrees per day in an inertial reference frame. It has been recognized by Roberson [Ref. 52], Doolin [Ref. 53], and others that the gradient of the earth's gravitational field can produce torques on a satellite which may result in a precession of the spin axis. An order of magnitude calculation of these gravity torques, using Roberson's results, was made. The torques were time averaged over a tumble cycle and then time averaged over an orbital period. The resulting average torque was about 16 dyne-cm assuming an orientation of the tumble axis that would produce the maximum effect. Since the moment of inertia about the transverse axis is about 5×10^7 gm cm² and the tumble rate is approximately 1 rad/sec, the angular momentum is 5×10^7 gm cm² sec⁻¹. A change in orientation of 10 degrees or .17 rad represents an angular momentum change of $.85 \times 10^7$ gm cm² sec⁻¹. For this change to occur in one day or 86,400 seconds requires a continuous torque on the order of 10^2 dyne-cm. This exceeds the gravitational torques by a factor of six.

Other effects that may give rise to precessing torques were examined cursorily. Aerodynamic forces near perigee will produce precessing torques due to the displacement of the center of lateral area from the center of gravity. The drag force at perigee, assuming an area of 3×10^3 cm², an atmospheric density of 10^{-13} gm cm⁻³, a velocity of 8×10^5 cm sec⁻¹, and a drag coefficient of two, is about 200 dynes. Assuming a ten cm displacement between the center of area and center of gravity, the resultant torque is on the order of 2000 dyne-cm. However, this torque is only effective for the small percentage of time during an orbital revolution when the satellite is near perigee. Furthermore, after the satellite has begun tumbling in a plane, it would appear that this torque would average to zero over a tumble cycle.

Interactions of a magnetic moment of the satellite with the geomagnetic field may give rise to precessing torques. If this magnetic moment is due to eddy currents induced by the tumbling motion of the satellite, the torques produced must be dissipative in nature. It has been established that the tumble rate changes by only 2×10^{-8} rad sec⁻² which corresponds to torques on the order of one dyne-cm. Therefore, the eddy currents appear to be much too small to produce the observed precessions.

No measurements have been made on Explorer IV to determine whether or not it had a magnetic moment due to permanent magnetism, induced magnetism, or internal circuitry. Such measurements could be made on a spare payload and may or may not provide an explanation for the torques that appear to be acting on the satellite.

APPENDIX 1

The conservation of magnetic moment may be shown in the following manner. Starting with equation 10,

$$m \frac{dv_{||}}{dt} = -\mu \nabla_{||} B,$$

multiplication by $v_{||}$ gives

$$\frac{d}{dt} \left(\frac{1}{2} m v_{||}^2 \right) = -\mu \frac{dB}{dz} \frac{dz}{dt} = -\mu \frac{dB}{dt}.$$

Equation 5 is

$$\frac{mv_{\perp}^2}{2} = \mu B$$

or

$$\frac{d}{dt} \left(\frac{mv_{\perp}^2}{2} \right) = \mu \frac{dB}{dt} + B \frac{d\mu}{dt}.$$

If kinetic energy of the particle is conserved,

$$\frac{d}{dt} \left(\frac{mv_{||}^2}{2} \right) + \frac{d}{dt} \left(\frac{mv_{\perp}^2}{2} \right) = 0$$

and

$$-\mu \frac{dB}{dt} + \mu \frac{dB}{dt} + B \frac{d\mu}{dt} = 0;$$

hence, μ is constant with time.

APPENDIX 2

Equation 13,

$$\dot{\phi} \cos \theta = \frac{I_3}{I_1} \omega_3,$$

may also be derived by direct geometrical argument. Let the total angular momentum \vec{L} be along the z-axis. Let the body be rolling about I_3 with angular velocity ω_3 and precessing about \vec{L} with the precession rate $\dot{\phi}$ such that I_3 makes angle θ with \vec{L} . Since angular velocities may be resolved into components and since I_1 is perpendicular to I_3 , the instantaneous angular momentum about I_1 is $I_2 \dot{\phi} \sin \theta$. The angular momenta about I_1 and I_3 may be resolved into components along \vec{L} such that

$$I_1 \dot{\phi} \sin^2 \theta + I_3 \omega_3 \cos \theta = L,$$

and components perpendicular to \vec{L} such that

$$I_1 \dot{\phi} \sin \theta \cos \theta - I_3 \omega_3 \sin \theta = 0.$$

From the latter equation

$$\dot{\phi} \cos \theta = \frac{I_3 \omega_3}{I_1} .$$

REFERENCES

1. Stormer, C. , The Polar Aurora (Oxford at the Clarendon Press, 1955).
2. Alfven, H. , Cosmical Electrodynamics - (Oxford at the Clarendon Press, 1950).
3. Spitzer, L. , Physics of Fully Ionized Gases (New York: Interscience Publishers, Inc. , 1956).
4. Northrop, T. G. , and Teller, E. , "Stability of the Adiabatic Motion of Charged Particles in the Earth's Field," Phys. Rev. 117, p. 215 (1960).
5. This is a sufficient but not necessary condition. Particles may be reflected away from regions of increasing field even if magnetic moment is not strictly conserved.
6. Meredith, L. H. , Gottlieb, M. B. , and Van Allen, J. A. , "Direct Detection of Soft Radiation above 50 Km in the Auroral Zone," Phys. Rev. 97, pp. 201-205 (1955).
7. Ludwig, G. H. , "Cosmic Ray Instrumentation in the First U. S. Earth Satellite," Rev. Sci. Instr. 30, pp. 223-229 (1959).
8. Van Allen, J. A. , Ludwig, G. H. , Ray, E. C. , and McIlwain, C. E. , IGY Satellite Report Series No. 3, pp. 73-92 (1958).
9. Van Allen, J. A. , McIlwain, C. E. , Ludwig, G. H. , "Radiation Observations with Satellite 1958 Epsilon," J. Geophys. Res. 64, pp. 272-285 (1959).
10. Christofilos, N. C. , "The Argus Experiment," J. Geophys. Res. 64, pp. 869-875 (1959).
11. Van Allen, J. A. , McIlwain, C. E. , and Ludwig, G. H. , "Satellite Observations of Electrons Artificially Injected into the Geomagnetic Field." J. Geophys. Res. 64, pp. 877-891 (1959).
12. Allen, L. , Beavers, J. L. , Whitaker, W. A. , Welch, J. A. , and Walton, R. B. , "Project Jason Measurement of Trapped Electrons from a Nuclear Device by Sounding Rockets," J. Geophys. Res. 64, pp. 893-907 (1959).
13. Van Allen, J. A. , and Franck, L. A. , "Radiation Around the Earth to a Radial Distance of 107,400 Kilometers," Nature 183, pp. 430-434 (1959).

14. Van Allen, J. A. , and Franck, L. A. , "Radiation Measurements to 658,300 KM with Pioneer IV," Nature 184, pp. 219-224 (1959).
15. Vernov, S. N. , and Chudakov, A. E. , "Terrestrial Corpuscular Radiation and Cosmic Rays," Space Research, ed. Bijl (Amsterdam: North Holland Publishing Co. , pp. 751-796 1960).
16. Vernov, S. N. , et al. , "Radiation Measurements During the Flight of the Second Soviet Space Rocket," Space Research, pp. 845-851.
17. Freden, S. C. , White, R. S. , "Protons in the Earth's Magnetic Field," Phys. Rev. Letters 3, p. 9 (1959).
18. Arnoldy, R. , et al. , "Measurements of the Van Allen Radiation Belts During Geomagnetic Storms," Space Research, pp. 877-896.
19. Van Allen, J. A. , Lin, Wei Ching, "Outer Radiation Belt and Solar Proton Observations with Explorer VII During March-April 1960," State University of Iowa Report SUI 60-10 (1960).
20. Vernov and Chudakov, Space Research, p. 777.
21. Singer, S. F. , "Radiation Belt and Trapped Cosmic Ray Albedo," Phys. Rev. Letters 1, pp. 181-183 (1958).
22. Singer, S. F. , "Trapped Albedo Theory of the Radiation Belt," Phys. Rev. Letters 1, pp. 181-183 (1958).
23. Singer, S. F. , "Nature and Origin of the Earth's Radiation Belts." Space Research, pp. 797-820 (1960).
24. Northrop and Teller, Phys. Rev. 117, p. 216 (1960).
25. Allen, Beavers, Whitaker, Welch, J. Geophys. Res. 64, p. 900 (1959).
26. Van Allen, McIlwain, and Ludwig, J. Geophys. Res. 64, p. 887 (1959).
27. Van Allen, McIlwain, and Ludwig, J. Geophys. Res. 64, p. 279 (1959).
28. Van Allen, McIlwain, and Ludwig, J. Geophys. Res. 64, p. 887 (1959).
29. Van Allen, McIlwain, and Ludwig, J. Geophys. Res. 64, p. 878 (1959).
30. Pilkington, W. C. , "Vehicle Motion as Inferred from Radio-Field-Strength Records," JPL Ext. Rpt. No. 551, Calif. Inst. of Tech. , pp. 8-40 (1958).

31. Ibid. , Appendix C, pp. 70-91.
32. Goldstein, H. , Classical Mechanics, (Cambridge: Addison-Wesley Publishing Co.), p. 160 (1956).
33. Slater, J. C. , and Frank, N. H. , Mechanics , (New York: McGraw-Hill Book Co., Inc.), p. 112 (1947).
34. Barr, T. A. , "Explorer IV Antennas," Explorer IV - 1958 Epsilon Orbital Data Series, Issue I, (Joint report prepared by Smithsonian Astrophysical Observatory, Cambridge, Mass. , and Army Ballistic Missile Agency, Huntsville, Alabama) p. 3 (1958).
35. Fields, S. A. , "Body Motions of 1958 Epsilon," Army Ballistic Missile Agency Technical Memorandum, CL-TM-11-60(1), (1960).
36. Snoddy, W. C. , "Theoretical and Measured Temperature for Explorer IV," ABMA Technical Note, DV-TN-6-59 (1959).
37. Heller, G. , "Problems Concerning the Thermal Design of Explorer Satellites," IRE Trans. on Mil. Elec. , Vol. MIL-4, p. 109 (Apr-July 60).
38. Barr, Explorer IV 1958 Epsilon Orbital Data Series, Issue I, pp. 3-7.
39. Ratcliffe, J. A. , The Magneto-Ionic Theory, (Cambridge University Press) 1959.
40. Daniels, F. B. , and Bauer, S. J. , "The Ionospheric Faraday Effect and its Applications," J. Franklin Inst. 267, pp. 187-200 (1959).
41. Adams, R. M. , Explorer IV - 1958 Epsilon Orbital Data Series, Issue 6, (a joint report prepared by Smithsonian Astrophysical Observatory, Cambridge, Massachusetts and the Army Ballistic Missile Agency, Redstone Arsenal, Alabama, November, 1959).
42. Lautman, D. A. , Smithsonian Astrophysical Observatory, Cambridge, Mass. , private communication.
43. Whitney, C. A. , "Atmospheric Densities from Explorer IV," Smithsonian Institution Astrophysical Observatory, Special Report No. 18, p. 15, Table II (October, 1958).
44. Jacchia, L. G. , "Solar Effects on the Acceleration of Artificial Satellites," Smithsonian Institution Astrophysical Observatory Special Report No. 29, pp. 1 - 18 (September 21, 1959).

45. Shelton, R. D. , "A Counter Problem," ABMA Technical Note, DV-TN-14-59 (1959).
46. Shelton, R. D. , "The Determination of the Directional Distribution of Charged Particles Trapped in the Magnetic Field of the Earth," paper presented to the Committee of AGARD, Paris, France (May, 1959).
47. Conant, G. H. , "Magnetic Field and Satellite Velocity Tabulations," Explorer IV - 1958 Epsilon Orbital Data Series, Issue 6, p. 4.
48. Finch, H. F. , and Leaton, B. R. , "The Earth's Main Magnetic Field, Epoch 1955.0, "Mon. Notices of the Royal Astronomical Society, Geophysics Supp. 7, pp. 313-317 (1957).
49. Fields, "Body Motions of 1958 Epsilon," p. 19.
50. Shelton, "A Counter Problem," pp. 4-11.
51. Van Allen, McIlwain, and Ludwig, J. Geophys. Res. 64, p. 280.
52. Roberson, R. E. , and Tatistcheff, D. , "The Potential Energy of a Small Rigid Body in the Gravitational Field of an Oblate Spheroid," J. Franklin Inst. 262, p. 209 (1956).
53. Doolin, B. F. , "Gravity Torque on an Orbiting Vehicle," NASA Technical Note, TN-D-70, Ames Research Center, Moffet Field, Calif. (1960).

BIBLIOGRAPHY

Books

- Alfven, H. Cosmical Electrodynamics. Oxford at the Clarendon Press, 1950.
- Arnoldy, R. , Hoffman, R. , and Winckler, J. R. "Measurements of the Van Allen Radiation Belts During Geomagnetic Storms," Space Research. ed. H. K. Kallmann Bijl, Amsterdam: North Holland Publishing Co. , 1960 (Proceedings of the First International Space Science Symposium).
- Goldstein, H. Classical Mechanics. Cambridge: Addison-Wesley Publishing Company. 1956.
- Ratcliffe, J. A. The Magneto-Ionic Theory. Cambridge: Cambridge University Press, 1959.
- Singer, S. F. "Nature and Origin of the Earth's Radiation Belts," Space Research.
- Slater, J. C. , and Frank, N. H. Mechanics. New York: McGraw-Hill Book Co. , Inc. , 1947.
- Spitzer, L. Physics of Fully Ionized Gases. New York: Interscience Publishers, Inc. , 1956.
- Stormer, C. The Polar Aurora. Oxford at the Clarendon Press, 1955.
- Vernov, S. N. , and Chudakov, A. E. "Terrestrial Corpuscular Radiation and Cosmic Rays," Space Research.
- Vernov, S. N. , et al. "Radiation Measurements During the Flight of the Second Soviet Space Rocket," Space Research.

Journals and Periodicals

- Allen, L. , Beavers, J. L. , Whitaker, W. A. , Welch, J. A. , and Walton, R. B. "Project Jason Measurement of Trapped Electrons from a Nuclear Device by Sounding Rockets," J. Geophys. Res. 64, pp. 893-907 (1959).
- Christofilos, N. C. "The Argus Experiment," J. Geophys. Res. 64, pp. 869-875 (1959);
- Daniels, F. B. , and Bauer, S. J. "The Ionospheric Faraday Effect and Its Applications," J. Franklin Inst. 267, pp. 187-200 (1959).

- Finch, H. F. and Leaton, B. R. "The Earth's Main Magnetic Field, Epoch 1955.0," Mon. Notices of the Royal Astronomical Soc. Geophysics Supp. 7, pp. 313-317 (1957).
- Freden, S. C., and White, R. S. "Protons in the Earth's Magnetic Field," Phys. Rev. Letters 3, pp. 9-11 (1959).
- Heller, G. "Problems Concerning the Thermal Design of Explorer Satellites," IRE Tran. on Mil. Electronics, Vol. Mil-4, pp. 98-112 (April-July 1960).
- Ludwig, G. H. "Cosmic Ray Instrumentation in the First U. S. Earth Satellite," Rev. Sci. Instr. 30, pp. 223-229 (1959).
- Meridith, L. H., Gottlieb, M. B., and Van Allen, J. A. "Direct Detection of Soft Radiation Above 50 KM in the Auroral Zone," Phys. Rev. 97, pp. 201-205 (1955).
- Northrop, T. G., and Teller, E. "Stability of the Adiabatic Motion of Charged Particles in the Earth's Field," Phys. Rev. 117, pp. 215-225 (1960).
- Roberson, R. E., and Tatistcheff, D. "The Potential Energy of a Small Rigid Body in the Gravitational Field of an Oblate Spheroid," J. Franklin Inst. 262, pp. 209-214 (1956).
- Singer, S. F. "'Radiation Belt' and Trapped Cosmic Ray Albedo," Phys. Rev. Letters 1, pp. 171-173 (1958).
- Singer, S. F. "Trapped Albedo Theory of the Radiation Belt," Phys. Rev. Letters 1, pp. 181-183 (1958).
- Van Allen, J. A., and Frank, L. A. "Radiation Around the Earth to a Radial Distance of 107,400 Kilometers," Nature 183, pp. 430-434 (1959).
- Van Allen, J. A., and Frank, L. A. "Radiation Measurements to 658,300 KM with Pioneer IV," Nature 184, pp. 219-224 (1959).
- Van Allen, J. A., McIlwain, C. E., and Ludwig, G. H. "Radiation Observations with Satellite 1958 Epsilon," J. Geophys. Res. 64, pp. 272-285 (1959).
- Van Allen, J. A., McIlwain, C. E., and Ludwig, G. H. "Satellite Observations of Electrons Artificially Injected into the Geomagnetic Field," J. Geophys. Res. 64, pp. 877-891 (1959).

Reports and Documents •

- Adams, R. M. Explorer IV - 1958 Epsilon Orbital Data Series, Issue 6. 6-volume ephemeris prepared by Smithsonian Astrophysical Observatory, Cambridge, Mass. and Army Ballistic Missile Agency, Redstone Arsenal, Ala. (Nov, 1959).
- Barr, T. A. "Explorer IV Antennas," Explorer IV - 1958 Epsilon Orbital Data Series, Issue 1. (Aug. 11, 1958) p. 3.
- Conant, G. H. "Magnetic Field and Satellite Velocity Tabulations," Explorer IV - 1958 Epsilon Orbital Data Series, Issue 6. p. 4.
- Doolin, B. F. "Gravity Torques on an Orbiting Vehicle," NASA Tech. Note, TN-D-70, Ames Research Center, Moffet Field, Calif. (1960).
- Fields, S. A. "Body Motions of 1958 Epsilon," Army Ballistic Missile Agency (ABMA) Tech. Memo, CL-TM-11-60 (1) (1960).
- Jacchia, L. G. "Solar Effects on the Acceleration of Artificial Satellites," Smithsonian Astrophysical Observatory Special Rpt. No. 29, pp. 1-18 (1959).
- Pilkington, W. C. "Vehicle Motion as Inferred from Radio Field Strength Records," Jet Propulsion Lab. Ext. Rpt. No. 551, Calif. Inst. of Tech. (1958).
- Shelton, R. D. "A Counter Problem," ABMA Tech. Note, DV-TN-14-59 (1959).
- Shelton, R. D. "The Determination of the Directional Distribution of Charged Particles Trapped in the Magnetic Field of the Earth," paper presented to the Committee of AGARD, Paris, France (May, 1959).
- Snoddy, W. C. "Theoretical and Measured Temperatures of Explorer IV," ABMA Tech Note, DV-TN-6-59 (1959).
- Van Allen, J. A., Ludwig, G. H., Ray, E. C., and McIlwain, C. E., IGY Satellite Report Series No. 3, pp. 73-92 (1958).
- Van Allen, J. A., and Lin, W. C. "Outer Radiation Belt and Solar Proton Observations with Explorer VII During March-April 1960," State University of Iowa Report SUI 60-10 (1960).
- Whitney, C. A. "Atmospheric Densities from Explorer IV," Smithsonian Astrophysical Observatory, Special Rpt. No. 18, pp. 13-22 (1958).

Private Communication

Smithsonian Astrophysical Observatory, Cambridge, Mass. Personal discussion with
D. A. Lautman.

"The aeronautical and space activities of the United States shall be conducted so as to contribute . . . to the expansion of human knowledge of phenomena in the atmosphere and space. The Administration shall provide for the widest practicable and appropriate dissemination of information concerning its activities and the results thereof."

—NATIONAL AERONAUTICS AND SPACE ACT OF 1958

NASA SCIENTIFIC AND TECHNICAL PUBLICATIONS

TECHNICAL REPORTS: Scientific and technical information considered important, complete, and a lasting contribution to existing knowledge.

TECHNICAL NOTES: Information less broad in scope but nevertheless of importance as a contribution to existing knowledge.

TECHNICAL MEMORANDUMS: Information receiving limited distribution because of preliminary data, security classification, or other reasons.

CONTRACTOR REPORTS: Technical information generated in connection with a NASA contract or grant and released under NASA auspices.

TECHNICAL TRANSLATIONS: Information published in a foreign language considered to merit NASA distribution in English.

TECHNICAL REPRINTS: Information derived from NASA activities and initially published in the form of journal articles.

SPECIAL PUBLICATIONS: Information derived from or of value to NASA activities but not necessarily reporting the results of individual NASA-programmed scientific efforts. Publications include conference proceedings, monographs, data compilations, handbooks, sourcebooks, and special bibliographies.

Details on the availability of these publications may be obtained from:

SCIENTIFIC AND TECHNICAL INFORMATION DIVISION
NATIONAL AERONAUTICS AND SPACE ADMINISTRATION
Washington, D.C. 20546